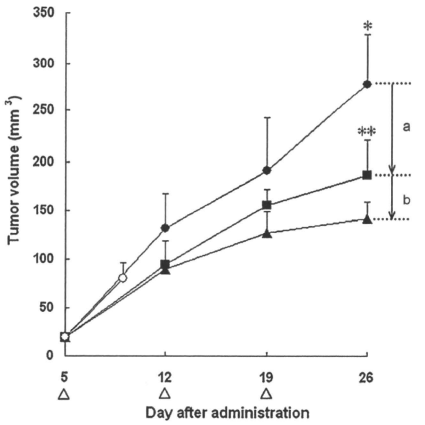

Fig. 9. Comparison of tumor growth suppression with CDDP-SLX-Lip, CDDP-Lip and CDDP in A549-bearing mice. Keys: ▲, CDDP-SLX-Lip (25 mg CDDP/kg body weight); ■,CDDP-Lip (25 mg CDDP/kg body weight); ○, CDDP solution (25 mg CDDP/kg body weight); ●, saline. Each sample was injected via tail veins of A549-bearing mice on days 5, 12 and 19 after tumor cell transplantation. At each day of 5, 12, 19 and 26 after transplantation, each tumor volume (mm^3) was measured. Each open triangle at the horizontal axis shows the time of administration. Results are expressed as the mean ± SD ($n = 4$). *$P < 0.01$ compared with saline. **$P < 0.05$ compared with CDDP-Lip. Vertical arrows indicate the effects of EPR (a) and active targeting (b).

derived vascular endothelial cell growth factor (VEGF) (Aoki et al., 2001), which could account for the enhanced antitumor activity of CDDP-SLX-Lip versus CDDP-Lip. CDDP-SLX-Lip might therefore be more effective than unconjugated CDDP on a wide range of tumors because a number of tumors are sensitive to VEGF-induced angiogenesis (Szekanecz et al., 1999).

Recently, the number of E-selectin-positive vessels was found to be higher in invasive micropapillary breast carcinoma than in invasive ductal carcinoma which was correlated with histological grade (Wei et al., 2008). Furthermore, TNF-α expression, which is known to induce E-selectin in vascular endothelial cells (Murakami et al., 2000), showed a significant positive correlation with the rate of proliferation, histological grade, lymph node metastasis and microvessel density (Cui et al., 2008). Targeting E-selectin should be a feasible and practical therapeutic strategy for breast carcinoma with poor prognosis. Further detailed studies such as distribution, clearance, toxicity, application for various tumor cells and doses with CDDP-SLX-Lip are underway.

5. Conclusion

We successfully established a novel efficient technology to encapsulate CDDP in liposomes at high concentrations. Targeting E-selectin on the vascular endothelial cells in tumor tissues by using CDDP-SLX-Lip should be effective in providing for selective tumor uptake.

The increased loading efficiency of CDDP together with the ability of targeting E-selectin are expected to enhance the pharmaceutical availability of CDDP and to improve the therapeutic index.

CDDP-SLX-Lip should provide a way of developing novel antitumor therapy with CDDP, decreasing the side effects without sparing the antitumor activity.

Acknowledgements

We thank Prof. T. Ema (Okayama University) for his kind support and helpful advises in measuring Pt content of CDDP by NMR and Prof. L. Fu (Tianjin Medical School) for helpful discussions.

References

Aoki, M., Kanamori, M., Yudoh, K., Ohmori, K., Yasuda, T., Kimura, T., 2001. Effects of vascular endothelial growth factor and E-selectin on angiogenesis in the murine metastatic RCT sarcoma. Tumour Biol. 22, 239–246.

Bandak, S., Goren, D., Horowitz, A., Tzemach, D., Gabizon, A., 1999. Pharmacological studies of cisplatin encapsulated in long-circulating liposomes in mouse tumor models. Anticancer Drugs 10, 911–920.

Bevilacqua, M.P., Stengelin, S., Gimbrone Jr., M.A., Seed, B., 1989. Endothelial leukocyte adhesion molecule 1: an inducible receptor for neutrophils related to complement regulatory proteins and lectins. Science 243, 1160–1165.

Borch, R.F., Markman, M., 1989. Biochemical modulation of cisplatin toxicity. Pharmacol. Ther. 41, 371–380.

Comis, R.L., 1994. Cisplatin: the future. Semin. Oncol. 21, 109–113.

Cui, L.F., Guo, X.J., Wei, J., Liu, F.F., Fan, Y., Lang, R.G., Gu, F., Zhang, X.M., Fu, L., 2008. Overexpression of TNF-α and TNFRII in invasive micropapillary carcinoma of the breast: clinicopathological correlations. Histopathology 53, 381–388.

Cvitkovic, E., Spaulding, J., Bethune, V., Martin, J., Whitmore, W.F., 1977. Improvement of *cis*-dichlorodiammineplatinum therapeutic index in an animal model. Cancer 39, 1357–1361.

Dhara, S., 1970. A rapid method for the synthesis of *cis*-[$Pt(NH_3)Cl_2$]. Indian J. Chem. 7, 193–194.

Drummond, D.C., Meyer, O., Hong, K., Kirpotin, D.B., Papahadjopoulos, D., 1999. Optimizing liposomes of chemotherapeutic agents to solid tumors. Pharmacol. Rev. 51, 691–743.

Gabizon, A.A., 1992. Selective tumor localization and improved therapeutic index of anthracyclines encapsulated in long-circulating liposomes. Cancer Res. 52, 891–896.

Goldstein, R.S., Noordewier, B., Bond, J.T., Hook, J.B., Mayor, G.H., 1981. *cis*-Dichlorodiammineplatinum nephrotoxicity: time course and dose response of renal functional impairment. Toxicol. Appl. Pharmacol. 60, 163–175.

Harrington, K.J., Lewanski, C.R., Northcote, A.D., Whittaker, J., Wellbank, H., Vile, R.G., Peters, A.M., Stewart, J.S., 2001. Phase I–II study of pegylated liposomal cisplatin (SPI-077) in patients with inoperable head and neck cancer. Ann. Oncol. 12, 493–496.

Hayes, D.M., Cvitkovic, E., Golbey, R.B., Scheiner, E., Helson, L., Krakoff, I.H., 1977. High dose *cis*-platinum diammine dichloride: amelioration of renal toxicity by mannitol diuresis. Cancer 39, 1372–1381.

Hirai, M., Minematsu, H., Kondo, N., Oie, K., Igarashi, K., Yamazaki, N., 2007a. Accumulation of liposome with Sialyl Lewis X to inflammation and tumor region: application to in vivo bio-imaging. Biochem. Biophys. Res. Commun. 353, 553–558.

Hirai, M., Oie, K., Igarashi, K., 2007b. In vivo imaging reagent with liposome with sugar chain. Med. Sci. Digest. 33, 826–828.

Huang, S.K., Mayhew, E., Gilani, S., Lasic, D.D., Martin, F.J., Papahadjopoulos, D., 1992. Pharmacokinetics and therapeutics of sterically stabilized liposomes in mice bearing C-26 colon carcinoma. Cancer Res. 52, 6774–6781.

Huang, S.K., Martin, F.J., Jay, G., Vogel, J., Papahadjopoulos, D., Friend, D.S., 1993. Extravasation and transcytosis of liposomes in Kaposi's sarcoma-like dermal lesions of transgenic mice bearing the HIV tat gene. Am. J. Pathol. 143, 10–14.

Kim, E.S., Lu, C., Khuri, F.R., Tonda, M., Glisson, B.S., Liu, D., Jung, M., Hong, W.K., Herbst, R.S., 2001. A phase II study of STEALTH cisplatin (SPI-077) in patients with advanced non-small cell lung cancer. Lung Cancer 34, 427–432.

Lee, C.M., Tanaka, T., Murai, T., Kondo, M., Kimura, J., Su, W., Kitagawa, T., Ito, T., Matsuda, H., Miyasaka, M., 2002. Novel chondroitin sulfate-binding cationic liposomes loaded with cisplatin efficiently suppress the local growth and liver metastasis of tumor cells in vivo. Cancer Res. 62, 4282–4288.

Legha, S.S., Hodges, C., Ring, S., 1992. Efficacy of ondansetron against nausea and vomiting caused by dacarbazine containing chemotherapy. Cancer 70, 2018–2020.

Liu, F.T., Rabinovich, G.A., 2005. Galectins as modulators of tumor progression. Nat. Rev. Cancer 5, 29–41.

Matsumura, Y., Maeda, H., 1986. A new concept for macromolecular therapeutics in cancer chemotherapy: mechanism of tumoritropic accumulation of proteins and the antitumor agent smancs. Cancer Res. 46, 6387–6392.

Mayer, B., Spatz, H., Funke, I., Johnson, J.P., Schildberg, F.W., 1998. De novo expression of the cell adhesion molecule E-selectin on gastric cancer endothelium. Langenbeck's Arch. Surg. 383, 81–86.

Meerum Terwogt, J.M., Groenewegen, G., Pluim, D., Maliepaard, M., Tibben, M.M., Huisman, A., ten Bokkel Huinink, W.W., Schot, M., Welbank, H., Voest, E.E., Beijnen, J.H., Schellens, J.M., 2002. Phase I and pharmacokinetic study of SPI-77, a liposomal encapsulated dosage form of cisplatin. Cancer Chemother. Pharmacol. 49, 201–210.

Murakami, T., Mataki, C., Nagao, C., Umetani, M., Wada, Y., Ishii, M., Tsutsumi, S., Kohro, T., Saiura, A., Aburatani, H., Hamakubo, T., Kodama, T., 2000. The gene expression profile of human umbilical vein endothelial cells stimulated by tumor necrosis factor alpha using DNA microarray analysis. J. Atheroscler. Thromb. 7, 39–44.

Navari, R.M., Kaplan, H.G., Gralla, R.J., Grunberg, S.M., Palmer, R., Fitts, D., 1994. Efficacy and safety of granisetron, a selective 5-hydroxytryptamine-3 receptor antagonist, in the prevention of nausea and vomiting induced by high-dose cisplatin. Clin. Oncol. 12, 2204–2210.

Newman, M.S., Colbern, G.T., Working, P.K., Engbers, C., Amantea, M.A., 1999. Comparative pharmacokinetics, tissue distribution, and therapeutic effectiveness of cisplatin encapsulated in long-circulating, pegylated liposomes (SPI-077) in tumor-bearing mice. Cancer Chemother. Pharmacol. 43, 1–7.

Ogilvie, G.K., Fettman, M.J., Jameson, V.J., Walters, L.M., Lafferty, M.H., Cooper, M.F., Powers, B.E., Ciekot, P.A., Atwater, S.W., Withrow, S.J., 1992. Evaluation of a one-hour saline diuresis protocol for administration of cisplatin to dogs. Am. J. Vet. Res. 53, 1666–1669.

Rosenberg, B., 1978. Platinum complex–DNA interactions and anticancer activity. Biochimie 60, 859–867.

Szekanecz, Z., Halloran, M.M., Haskell, C.J., Shah, M.R., Polverini, P.J., Koch, A.E., 1999. Mediators of angiogenesis: the role of cellular adhesion molecules. Trends Glycosci. Glycotechnol. 11, 73–93.

Vaage, J., Donovan, D., Wipff, E., Abra, R., Colbern, G., Uster, P., Working, P., 1999. Therapy of a xenografted human colonic carcinoma using cisplatin or doxorubicin encapsulated in long-circulating pegylated stealth liposomes. Int. J. Cancer 80, 134–137.

Veal, G.J., Griffin, M.J., Price, E., Parry, A., Dick, G.S., Little, M.A., Yule, S.M., Morland, B., Estlin, E.J., Hale, J.P., Pearson, A.D., Welbank, H., Boddy, A.V., 2001. A phase I study in paediatric patients to evaluate the safety and pharmacokinetics of SPI-77, a liposome encapsulated formulation of cisplatin. Br. J. Cancer 84, 1029–1035.

Vestweber, D., Blanks, J.E., 1999. Mechanisms that regulate the function of the selectins and their ligands. Physiol. Rev. 79, 181–213.

Von Hoff, D.D., Schilsky, R., Reichert, C.M., Reddick, R.L., Rozencweig, M., Young, R.C., Muggia, F.M., 1979. Toxic effects of *cis*-dichlorodiammineplatinum (II) in man. Cancer Treat. Rep. 63, 1527–1531.

Wei, J., Cui, L., Liu, F., Fan, Y., Lang, R., Gu, F., Guo, X., Tang, P., Fu, L., 2008. E-selectin and Sialyl Lewis X expression is associated with lymph node metastasis of invasive micropapillary carcinoma of the breast. Int. J. Surg. Pathol. [Epub ahead of print].

Wu, N.Z., Da, D., Rudoll, T.L., Needham, D., Whorton, A.R., Dewhirst, M.W., 1993. Increased microvascular permeability contributes to preferential accumulation of Stealth liposomes in tumor tissue. Cancer Res. 53, 3765–3770.

Yamazaki, N., 1989. Analysis of the carbohydrate-binding specificity of lectin-conjugated lipid vesicles, which interact with polysaccharide, fragments. J. Membr. Sci. 41, 249–267.

Yamazaki, N., Kodama, M., Gabius, H.-J., 1994. Neoglycoprotein–liposome and lectin–liposome conjugates as tools for carbohydrate recognition research. Methods Enzymol. 242, 56–65.

Biotechnol Lett (2010) 32:361–366
DOI 10.1007/s10529-009-0160-9

ORIGINAL RESEARCH PAPER

Production of biologically active IgG hinge-tag soluble epidermal growth factor receptors (ErbB)

Takayuki Otani · Toshihiro Hashizume · Tadahiro Nagaoka · Tomoko Fukuda · Careen K. Tang · David S. Salomon · Masaharu Seno

Received: 15 September 2009 / Revised: 18 October 2009 / Accepted: 22 October 2009 / Published online: 7 November 2009

Abstract The extracellular domains (ECD) of epidermal growth factor receptors, ErbB1, 2, 3 and 4, were designed as soluble dimeric forms. Each ECD was fused to a short hinge region derived from IgG, such that the stable dimer could be formed with disulfide bridges. This hinge-tagged design minimized the molecular weight to approximately 50% of the conventional Fc-fusion design without an Fc domain of IgG. The refolded dimers could be easily analyzed and characterized by SDS-PAGE. Hinge-tagged soluble ErbBs demonstrated significant affinity for betacellulin and heregulin. The IgG hinge-tag should be a simple method to design soluble dimers that would be useful for high throughput screening of ligands, antagonists or derivatives.

Keywords Epidermal growth factor receptors · ErbB · Extracellular domain · Hinge region · Homodimer · Soluble receptor

Takayuki Otani, Toshihiro Hashizume and Tadahiro Nagaoka equally contributed to this paper.

T. Otani · T. Hashizume · T. Fukuda · M. Seno (✉)
Department of Medical and Bioengineering Science, Graduate School of Natural Science and Technology, Okayama University, 3.1.1 Tsushima-Naka, Kita-ku, Okayama 700-8530, Japan
e-mail: mseno@cc.okayama-u.ac.jp

T. Nagaoka · D. S. Salomon
Tumor Growth Factor Section, Mammary Biology & Tumorigenesis Laboratory, Center for Cancer Research, National Cancer Institute, National Institutes of Health, Bethesda, MD 20892, USA

C. K. Tang
Lombardi Comprehensive Cancer Center, Georgetown University, Washington, DC 20057, USA

Introduction

The epidermal growth factor (EGF) receptor family consists of four members, the EGF receptor (ErbB1), ErbB2, ErbB3, and ErbB4 (Holbro et al. 2003). These receptors play important roles in cellular differentiation, proliferation, transformation and tumorigenesis (Hynes et al. 2001). Each ErbB receptor is a type I transmembrane tyrosine kinase consisting of an extracellular domain (ECD), a transmembrane region and a cytoplasmic domain, which possess tyrosine kinase activity and which is responsible for intracellular signal transduction (Schlessinger 2000). Each ErbB ECD exhibits high affinity to peptides of the EGF-related growth factors that include EGF, TGFα, heregulins (HRG), amphiregulin, betacellulin (BTC), heparin-binding EGF like growth factor (HB-EGF), epiregulin and epigen (Linggi and Carpenter 2006). Upon ligand binding, ErbB receptors undergo homo- and/or hetero-dimerization to induce the intrinsic receptor tyrosine kinase activity, which ultimately results in the simulation of series of intracellular signaling cascades. Soluble ErbB receptors (sErbBs),

which are useful for screening the specificity and the cell surface affinity for ligands and which can inhibit ligands from binding to cognate receptors, have previously been synthesized as proteins between the fusion of the ECD and the Fc domain of IgG (Chamow and Ashkenazi 1996; Fitzpatrick et al. 1998; Jones et al. 1999). Fusion of the Fc domain to the ECD facilitates stable dimer formation which can be purified by affinity chromatography with a protein A coupled gel matrix. However, it is extremely difficult to distinguish dimers from higher order oligomers by conventional SDS-PAGE due to the high molecular weight of the oligomers of the ECD fused to the Fc domain. In this study, we have employed the short hinge region of the Fc domain, which is responsible for the intermolecular disulfide bridges of IgG molecule. This fragment was fused to each of the ECDs of the four ErbBs. The ECD of ErbB1 bound to EGF has the potential for self-dimerization without the transmembrane and cytoplasmic domains (Odaka et al. 1997). Similarly, the ECD of ErbB1 and the ECD of ErbB4 are able to form ligand-activated homodimers in solution (Ferguson et al. 2000). These two reports lead us to assess whether the whole Fc domain of IgG is actually necessary to facilitate dimerization of the ECDs of ErbBs.

Materials and methods

Construction of expression plasmids

cDNAs for the ECD of the ErbB2 and ErbB3 were cloned by RT-PCR from the total RNA of human breast tumor (Clontech) into pCR2.1vector (Invitrogen) respectively. The fragments coding for each ECD were subcloned into pEGFP-N1 (Stratagene) with a FLAG tag epitope. To design sErbB2 and sErbB3 in a dimeric form exploiting disulfide bounds between each hinge region, a synthetic oligo-nucleotide coding for the hinge region of the mouse IgG1 heavy chain (GenBank J00453) 5′-CCGGTGCCCAGGGATTCT GGTTGTAAGCCTTGCATATGTGTA-3′ was inserted into sErbB2-FLAG and sErbB3-FLAG and the expression plasmids for sErbB2-hinge-FLAG and sErbB3-hinge-FLAG were constructed. Human HRGβ2 cDNA was previously described by Tang et al. (1996). To create the expression plasmid for His-HRGβ2-HA, the portion encoding amino acid residues 176–241 corresponding to the EGF motif was inserted into pET14b (Novagen) together with a synthetic oligonucleotide coding for the HA-tag derived from the human influenza hemagglutinin protein. sErbB1 and sErbB4 fused to mouse IgG_1 heavy chain hinge region and His-BTC-HA were described by Nagaoka et al. (2008) in a similar design.

Expression and purification of sErbBs

Either Cos7 cells or HEK293H cells (Gibco) were transformed with each sErbB-hinge-Flag expression plasmid. Transient transformants of Cos7 cells were cultured for 2 days under low serum condition. Transformants of HEK293H cells stably expressing sErbBs were cultured in DMEM containing 30 mM HEPES, pH 7.5, 5% Daigo's GF21 (Nihon Pharmaceutical), 0.5 mg G418/ml and 0.05% Pluronic F-68 (Sigma-Aldrich) at 37°C for 5 days. The cells were then maintained in culture for an additional 5 days in fresh medium. Each sErbB in the medium was purified with an anti-FLAG agarose (Sigma-Aldrich) affinity column. The adsorbed protein was eluted with 0.1 M sodium phosphate buffer, pH 3.5, and the eluted fraction was neutralized with 2 M sodium phosphate buffer, pH 8.0. The buffer was then replaced with PBS by a PD-10 desalting column (GE Healthcare).

Expression and purification of His-HRGβ2-HA and His-BTC-HA

E. coli MM294 (DE3) pLysS (Watanabe et al. 1990) was transformed with the expression vector of His-HRGβ2-HA or His-BTC-HA and each recombinant protein was produced as inclusion bodies. The isolation of inclusion bodies and refolding of the protein was performed as described by Nagaoka et al. (2008). The refolded proteins were purified with a Ni-NTA Superflow column (Qiagen) following the procedure recommended by the manufacturer. The final purity of recombinant protein was evaluated by SDS-PAGE stained with Coomassie Brilliant Blue.

Enzyme immunoassay

The enzyme immunoassay (EIA) was designed to evaluate the affinity of ligands to sErbBs. Each well of a 96-well plate was coated with 100 ng BTC or HRGβ2. Then sErbBs sequentially diluted with PBSB

was added to each well followed by the incubation for 2 h at room temperature. The bound sErbBs were detected with anti-FLAG bioM2 monoclonal antibody coupled with Avidin-HRP conjugate (Zymed Laboratories). The HRP reaction was developed with *o*-phenylenediamine and H_2O_2. After the quench of reaction, absorbance at 492 nm of each well was measured. Each experiment was performed in triplicate.

Competition EIA to estimate Kd value

To estimate dissociation constants (Kd) between HRGβ2 and sErbB3 or sErbB4, competition EIA was performed based on the method described by (Djavadi-Ohaniance et al. 1996). Each well of a 96-well plate was coated with 50 ng HRGβ2. sErbBs were then premixed with varying concentrations of HRGβ2 and added to the wells. The bound sErbBs were detected with HRP labeled anti-FLAG-HRP monoclonal antibody. The HRP reaction was developed with OPD and hydrogen peroxide. After the quench of reaction, absorbance at 492 nm of each well was measured. Each experiment was performed in triplicate.

Western blotting

Proteins were resolved by 5% (v/v) SDS-PAGE and transferred to a PVDF membrane (Bio-Rad). Blots were then probed with anti-FLAG bioM2 monoclonal antibody, anti-HA-tag monoclonal antibody (Roche) or anti-His-tag monoclonal antibody (Cell Signaling) coupled with HRP conjugated Avidin, protein A-HRP (ICN Biomedicals) or anti-mouse IgG polyclonal antibody (Bio-Rad). The HRP signal was developed with Western Lighting and Western Lighting Plus Chemiluminescence Reagent (Perkin Elmer) and exposed to X-ray film (Fuji Film).

Results and discussion

The design of sErbB receptors tagged with the hinge region of mouse IgG tethered to a FLAG-tag epitope is summarized in Fig. 1. When sErbB receptors are designed as a conventional Fc fusion proteins, the molecular weight of the fusion proteins are approximately 120 kDa and the dimers are 240 kDa as listed in Table 1. It is difficult to distinguish these high molecular weight species in conventional procedures such as SDS-PAGE or gel filtration chromatography. In addition, if oligomeric forms are present, it would be even more difficult to distinguish these forms from dimers. On the other hand, the size of the sErbB-hinge-FLAG construct is approx. 70 kDa, which can generate a 140 kDa dimer. These sizes permit for sufficient resolution on SDS-PAGE analysis under non-reducing conditions (Fig. 2a). The size of the hinge-tag region that is fused to each soluble receptor is 1.7 kDa, so that it should not affect the overall size of the ECD (Table 1). Likewise, this construct does not significantly affect the size such that the dimeric forms of each ErbB receptor can be easily resolved and characterized by SDS-PAGE analysis. When the sErbBs that were fused to FLAG-tag with/without the hinge-tag region produced in the culture medium were immunoprecipitated with anti-FLAG antibody, sErbB1, 3 and 4 were found to successfully form dimers only when they were fused to the IgG hinge-tag

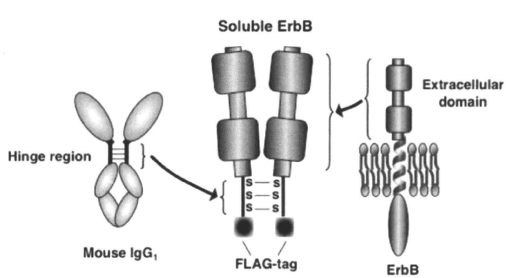

Fig. 1 Schematic drawing of soluble ErbBs with hinge-tag. Hinge region of a mouse IgG_1 was fused to the *C*-terminus of extracellular domain of ErbBs so that they should dimerize into a soluble form via disulfide bridges. Hinge-tag is followed by FLAG-tag at the *C*-terminus for easy detection of the molecule

Table 1 Comparison of molecular weights of sErbB-HF and sErbB-Fc

	Whole (kDa)	ECD (kDa)	sErbB-Fc[a] (kDa)	sErbB-HF[b] (kDa)
ErbB1				
Monomer	132	68.6	118.6	70.3
Homodimer	264	137.2	237.2	140.6
ErbB2				
Monomer	136	69.4	119.4	71.1
Homodimer	272	138.8	238.8	142.2
ErbB3				
Monomer	146	68.7	118.7	70.4
Homodimer	292	137.4	237.4	140.8
ErbB4				
Monomer	145	69.8	119.8	71.5
Homodimer	290	139.6	239.6	143.0

[a] sErbB fused to IgG Fc domain

[b] sErbB fused to hinge-tag and FLAG-tag

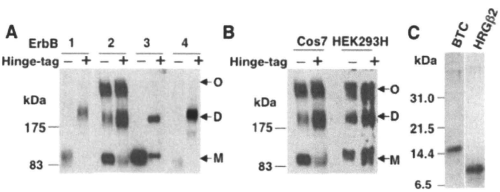

Fig. 2 **a** sErbBs with/without hinge-tags expressed in Cos7 cells. **b** Comparison of sErbB2 produced in Cos7 cells and HEK293H cells. sErbBs in the conditioned media were immunoprecipitated by anti-FLAG agarose and subjected to 5% SDS-PAGE under non-reduced conditions and transferred to PVDF membrane. The blots were probed with anti-FLAG Bio M2 antibody. The positions of monomers (M), dimers (D) and oligomers (O) are shown with *arrows*. **c** Recombinant BTC or HRGβ2 proteins purified to a homogeneity. BTC (MW = 9 kDa) and HRGβ2 (MW = 10 kDa) were produced in *E. coli* with His-tag and HA-tag, purified by Ni-column and subjected to SDS-PAGE under reduced condition. Coomassie Brilliant Blue staining

(Fig. 2a). Although sErbB2 showed oligomeric forms without the hinge-tag region, dimerization of sErbB2 was significantly enhanced with the hinge-tag (Fig. 2a). The oligomeric forms of sErbB2 were observed independently of the cell type, in which they were expressed (Fig. 2b). These oligomeric forms of ErbB2 can easily be reduced to dimeric forms during the purification procedure (data not shown) suggesting that the conformation of the extracellular domain of ErbB2 on the cell surface is labile. This flexible conformation might be a part of conditions that control signal transduction of ErbB2, of which dimerization is independent of ligand binding, resulting in a poor prognosis of cancers when ErbB2 is overexpressed.

For the evaluation of the affinity of the sErbBs to different ligands, recombinant BTC and HRGβ2 were expressed in bacteria and purified to near homogeneity as shown in Fig. 2c. BTC bound to both sErbB1 and sErbB4 in a similar manner (Fig. 3a). HRGβ2 bound to both sErbB3 and sErbB4 showing higher saturation binding to sErbB4 than sErbB3 (Fig. 3b). These ligands did not bind to sErbBs without the hinge-tag region (data not shown). From competition EIA, Kd values for HRGβ2 binding to sErbB3 and sErbB4 were estimated 111 and 51 nM, respectively. These Kd values are close to those previously reported (Fitzpatrick et al. 1998; Jones et al. 1999; Ferguson et al. 2000; Bouyain et al. 2005). Table 2 summarizes Kd values of the ligands and sErbBs together with those described previously. These results suggest that sErbB dimers with hinge-tag have significant binding affinity for BTC and HRGβ2 while the artificial and structurally unrelated peptide ligand EC-1 showed low affinity for sErbB2 (Hashizume et al. 2008). Therefore the full

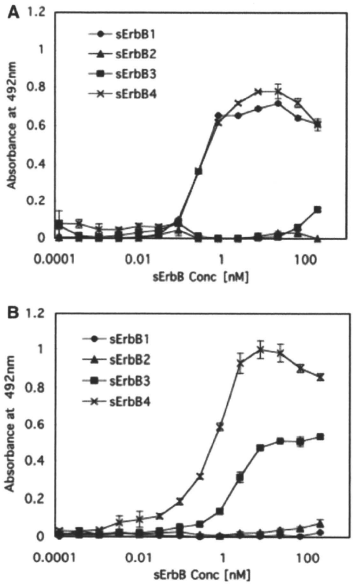

Fig. 3 Binding saturation of BTC (**a**) and HRGβ2 (**b**) assessed by enzyme immunoassay with hinge-tagged sErbBs. Ligands were coated at 100 ng/well in 96 well plate and varying concentration of sErbBs was added. Bound sErbBs were detected with biotinylated anti-FLAG antibody and HRP-avidin. SD was calculated from three independent experiments. Kd values of them were summarized in Table 2

Table 2 Kd values of BTC or HRGβ2 and receptors interaction

Ligand	Kd (nM)			
	sErbB1	sErbB2	sErbB3	sErbB4
BTC	0.35	N.D.[a]	N.D.	3.2
HRGβ2	N.D.	N.D.	111	51
EC-1[b]	N.D.	1.0×10^3	N.D.	N.D.

[a] No significant binding between ligand and sErbB was detected. These results are consistent with the facts that BTC specifically binds to ErbB1 and ErbB4, that HRGβ2 specifically binds to ErbB3 and ErbB4, and that neither of the two binds to ErbB2

[b] Hashizume et al. (2008)

length of Fc domain of IgG is not necessary for the dimerization of the sErbBs and the hinge-tag region should be effective to facilitate sErbB dimerization. These sErbB receptors should be useful for high throughput screening of ligands, antagonists or derivatives.

Acknowledgements We thank Ms. N. Hironaka for the construction of sErbB2 and sErbB3 expression plasmid. This research was partly supported by the Ministry of Education, Culture, Sports, Science and Technology Grant-in-Aid for Scientific Research (B) Nos. 18300164 and 21300179.

References

Bouyain S, Longo PA, Li S, Ferguson KM et al (2005) The extracellular region of ErbB4 adopts a tethered conformation in the absence of ligand. Proc Natl Acad Sci USA 102:15024–15029

Chamow SM, Ashkenazi A (1996) Immunoadhesins: principles and applications. Trends Biotechnol 14:52–60

Djavadi-Ohaniance L, Goldberg ME, Friguet B (1996) Measuring antibody affinity in solution. In: McCafferty J, Hoogenboom HR, Chiswell DJ (eds) Antibody engineering: a practical approach. IRL Press, Oxford, pp 77–98

Ferguson KM, Darling PJ, Mohan MJ et al (2000) Extracellular domains drive homo- but not hetero-dimerization of ErbB receptors. EMBO J 19:4632–4643

Fitzpatrick VD, Pisacane PI, Vandlen RL et al (1998) Formation of a high affinity heregulin binding site using the soluble extracellular domains of ErbB2 with ErbB3 or ErbB4. FEBS Lett 431:102–106

Hashizume T, Fukuda T, Nagaoka T et al (2008) Cell type dependent endocytic internalization of ErbB2 with an artificial peptide ligand that binds to ErbB2. Cell Biol Int 32:814–826

Holbro T, Civenni G, Hynes NE (2003) The ErbB receptors and their role in cancer progression. Exp Cell Res 284:99–110

Hynes NE, Horsch K, Olayioye MA et al (2001) The ErbB receptor tyrosine family as signal integrators. Endocr Relat Cancer 8:151–159

Jones JT, Akita RW, Sliwkowski MX (1999) Binding specificities and affinities of EGF domains for ErbB receptors. FEBS Lett 447:227–231

Linggi B, Carpenter G (2006) ErbB receptors: new insights on mechanisms and biology. Trends Cell Biol 16:649–656

Nagaoka T, Fukuda T, Hashizume T et al (2008) A betacellulin mutant promotes differentiation of pancreatic acinar AR42J cells into insulin-producing cells with low affinity of binding to ErbB1. J Mol Biol 380:83–94

Odaka M, Kohda D, Lax I et al (1997) Ligand-binding enhances the affinity of dimerization of the extracellular domain of the epidermal growth factor receptor. J Biochem 122:116–121

Schlessinger J (2000) Cell signaling by receptor tyrosine kinases. Cell 103:211–225

Tang CK, Perez C, Grunt T et al (1996) Involvement of heregulin-β2 in the acquisition of the hormone-independent phenotype of breast cancer cells. Cancer Res 56:3350–3358

Watanabe T, Seno M, Sasada R et al (1990) Molecular characterization of recombinant human acidic fibroblast growth factor produced in *E. coli*: comparative studies with human basic fibroblast growth factor. Mol Endocrinol 4:869–879

Journal of Controlled Release 149 (2011) 29–35

Contents lists available at ScienceDirect

Journal of Controlled Release

journal homepage: www.elsevier.com/locate/jconrel

Acylation of octaarginine: Implication to the use of intracellular delivery vectors

Sayaka Katayama, Hisaaki Hirose, Kentaro Takayama, Ikuhiko Nakase, Shiroh Futaki *

Institute for Chemical Research, Kyoto University, Uji, Kyoto 611-0011, Japan

ARTICLE INFO

Article history:
Received 18 November 2009
Accepted 1 February 2010
Available online 6 February 2010

Keywords:
Arginine-rich peptide
Cell-penetrating peptide
Fatty acid
Membrane interaction

ABSTRACT

Cell-penetrating peptides (CPPs) have the ability to efficiently internalize into cells and thus have been used as a vector for the intracellular delivery of various bioactive molecules. The introduction of a hydrophobic core to CPPs may increase their interaction with membranes and facilitate their translocation into cells. While the usefulness of acylated oligoarginine to gene and siRNA delivery has been largely reported, little information is available about their use for the delivery of small molecular-weight compounds, peptides and proteins. In this report, we employed octaarginine (R8) as a typical arginine-rich CPP and evaluated the effect of acylation using butanoic, hexanoic and decanoic acids on its capacity as a delivery vector. Hexanoyl octaarginine (C6R8-Alexa) showed the highest efficiency of cellular uptake of the studied variants, ten times higher than R8-Alexa. C6R8-Alexa also produced a diffuse cytosolic distribution. On the other hand, a less significant effect of C6R8 over R8 was observed for the delivery of proteins, suggesting that the advantage of C6R8 may be obtained during the delivery of relatively small molecular-weight compounds. Although less prominent than at 37 °C, a significant cytosolic distribution of C6R8-Alexa was observed at 4 °C, and this suggested the potential ability of the C6R8 peptide for direct penetration through plasma membranes.

1. Introduction

While plasma membranes play a crucial function to maintain cellular structures and functions, they work as a strong barrier against the intracellular delivery of membrane-impermeable agents [1]. Arginine-rich cell-penetrating peptides (CPPs), such as HIV-1 TAT and octaarginine (R8), have been employed as a delivery vector of these agents into cells [2–5]. The contribution of endocytosis including macropinocytosis, a form of actin-driven and clathrin/caveola-independent endocytosis, has been reported for the cellular uptake of arginine-rich CPPs and their conjugates [6–10]. The cargo molecules taken up by the cells via endocytosis have to escape from endosomes to exert their biological activity in the cytosol and nucleus. One possible approach to improve the endosomal escape of the cargo molecules may be to introduce hydrophobic moieties onto peptides to increase their affinity to cell membranes (Fig. 1). Our previous study suggested that the increasing affinity of oligoarginines to a cell surface, e.g., increasing the number of arginines and removing serum proteins from the medium, would produce a change in the peptide uptake with a prominent cytosolic peptide distribution [11]. In addition, it has been demonstrated that an efficient intracellular delivery of genes and siRNA was achieved by the non-covalent complex formation of these molecules with stearyl and cholesteryl oligoarginines [12–14]. Improvement of efficiency in CPP-mediated delivery by lipidation has also been reported [15–17]. However, only limited information is available about the intracellular fate of the acylated oligoarginines and their applicability as a delivery vector for peptides/proteins as well as compounds of relatively small molecular weight.

In this study, using octaarginine (R8) peptides as a typical arginine-rich CPP, the effect of N-terminal acylation on cellular uptake was evaluated using fatty acids having various chain lengths (Table 1). The study using the Alexa488 labeled acylated CPPs showed that hexanolyl R8 (C6R8-Alexa) produced ten times greater cellular uptake by the HeLa cells with efficient spread of the peptide signals in the cytosol and nucleus. The internalization mechanisms, and scope and limitation of the peptide as a delivery vector were also discussed.

2. Results and discussion

2.1. Effect of acylation on cellular uptake of octaarginine

We first examined the effect of the fatty acid modification of octaarginine (R8) in terms of the total cellular uptake and cellular distribution. R8 modified with straight-chain fatty acids of different chain lengths, namely, butanoyl R8 (C4R8), hexanoyl R8 (C6R8), decanoyl R8 (C10R8), tetradecanoyl (myristoyl) R8 (C14R8), and octadecanoyl (stearyl) R8 (C18R8) were prepared by Fmoc-solid-

Abbreviations: R8, Octaarginine; C6R8, Hexanoyl octaarginine; FACS, Fluorescence-activated cell sorter; CLSM, Confocal laser scanning microscopy; PI, Propidium iodide; CytD, Cytochalasin D; Ub, Ubiquitin; CA, Carbonic anhydrase; EMCS, *N*-(6-malaimidocaproyloxy) succinimide; PAD, Proapoptotic domain peptide; α-MEM, α-minimum essential medium; RP-HPLC, Reverse phase high-performance liquid chromatography; MALDI-TOFMS, Matrix-assisted laser desorption ionization-time-of-flight mass spectrometry.

* Corresponding author. Tel.: +81 774 38 3210; fax: +81 774 32 3038.
E-mail address: futaki@scl.kyoto-u.ac.jp (S. Futaki).

0168-3659/$ – see front matter © 2010 Elsevier B.V. All rights reserved.
doi:10.1016/j.jconrel.2010.02.004

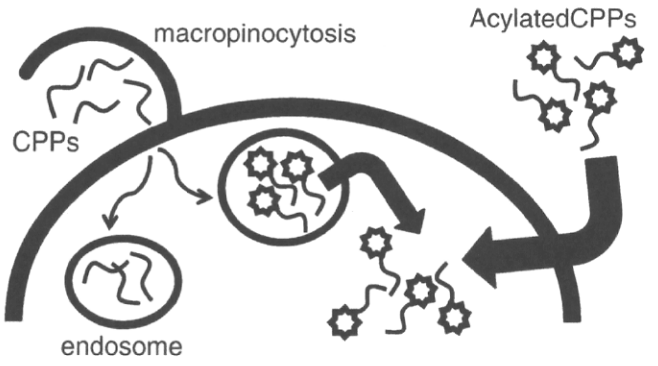

Fig. 1. Possible internalization routes of acylated CPPs. Acylation of arginine-rich CPPs may increase the interaction of the peptides with the membrane to facilitate the endosomal escape after their endocytic uptake or to promote direct penetration through the plasma membranes.

Table 1
Structures of the peptides used in this study.

Name	Fatty acid	Structure
R8	–	RRRRRRRRGC-amide
C4R8	Butanoic acid	C_3H_7CO-RRRRRRRRGC-amide
C6R8	Hexanoic acid	$C_5H_{11}CO$-RRRRRRRRGC-amide
C10R8	Decanoic acid	$C_9H_{19}CO$-RRRRRRRRGC-amide

phase peptide synthesis, and labeled with Alexa488 [CnR8-Alexa ($n=4$, 6, 10, 14, and 18, respectively)]. Alexa488 modification was conducted to assess peptide internalization by CLSM observation and FACS analysis. This fluorophore can also be regarded as a model of a small molecular-weight compound to be delivered into cells with the help of the peptide vector.

For CLSM analysis, HeLa cells were treated with 10 μM peptides at 37 °C for 30 min in α-minimum essential medium containing 10% serum [α-MEM(+)]. The cells treated with Alexa488-labeled R8 (R8-Alexa) showed punctate signals (Fig. 2A). This suggested that the fluorophore was taken up by the cells together with R8 via endocytosis and that the majority of the fluorophore was trapped in the endosomes without translocating into the cytosol as previously reported [7]. The C4R8-Alexa also yielded similar punctate signals in the cells. In contrast, C6R8-Alexa and C10R8-Alexa yielded diffuse signals throughout the cells together with punctate endosome-like signals. This suggested that the fluorophore was efficiently delivered into the cytosol and nucleus by conjugation with these peptides. Note that all the CLSM images in this study were obtained using live cells and the diffuse signals were not due to artifacts by fixation as previously pointed out [6]. Therefore, N-terminus acylation with hexanoic and decanoic acids effectively facilitated the translocation of R8-Alexa into the cytosol. Further elongation of the acyl chain lowered the solubility of the peptides, and it was difficult to treat the cells with C14R8-Alexa and C18R8-Alexa due to the formation of insoluble aggregates when applied to the culture media, thus no further study on their cellular uptake was conducted (data not shown).

FACS analysis of the cells treated with these conjugates showed that the use of C6R8 yielded the highest amount of total cellular uptake of the fluorophore (i.e., the sum of the fluorophore trapped in the endosomes and delivered into the cytosol). More than a 13-time

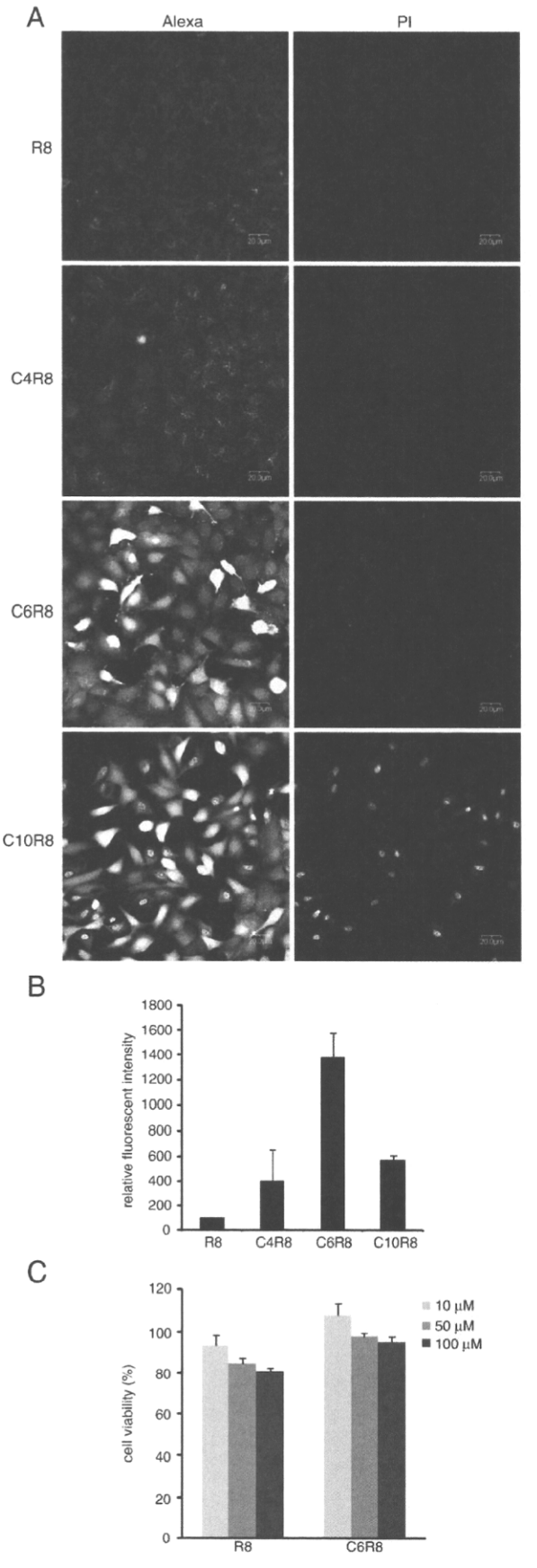

Fig. 2. CLSM analysis of the cells treated with acylated R8 peptides. (A) The HeLa cells were incubated with acylated R8 peptides labeled with Alexa488 (10 μM) in the presence of 5 μM propidium iodide (PI) for 30 min at 37 °C in α-MEM containing 10% serum [α-MEM(+)] prior to the CLSM analysis. Scale bar, 20 μm. (B) FACS analysis of the total cellular uptake of the acylated R8 peptides. The cells were treated with 10 μM peptides for 30 min at 37 °C in α-MEM(+) and the total cellular uptake was quantified. (C) Cytotoxicity analysis using the WST-1 assay. The HeLa cells were treated with non-labeled C6R8 or R8 for 24 h.

higher amount of the fluorophore was delivered into the cells using C6R8 than when using R8 as a vector (Fig. 2B). C10R8 produced an uptake of about 40% as much as that of C6R8. Although C4R8 produced endosome-like punctate signals of the fluorophore as in the case of R8, the total cellular uptake was about four times as much as the latter.

Enhanced cellular uptake of the fluorophore conjugated with acylated R8 may be attributed to the increased interaction between the peptides and membranes. On the other hand, the increasing membrane interaction or amphiphilicity of the peptide vectors may enhance membrane perturbation. This was assessed by coincubation of the acylated peptide vectors with a membrane-impermeable nuclear staining dye, propidium iodide (PI) (Fig. 2A, right panels). Perturbation of the plasma membranes would allow the dye to penetrate through the membranes resulting in nuclear staining. No significant nuclear staining was observed for the cells treated with 10 μM R8-, C4R8-, and C6R8-Alexa conjugates, suggesting very little effect of these vectors on the integrity of the plasma membranes under the given conditions. However, a considerable number of cells treated with C10R8-Alexa were PI positive. Excessive increase in the acyl chain length of the vectors would accompany the change in the surfactant effect of the vectors and thus produce a perturbation of the plasma membranes.

These results suggested the potential superiority of C6R8 over R8 as an intracellular delivery vector of compounds of relatively small molecular weight. The absence of a significant cytotoxicity of the C6R8 was further confirmed. To avoid the possible toxicity caused by the Alexa488 moiety, HeLa cells were treated with C6R8 without Alexa labeling ($C_5H_{11}CO$-R8-amide), and viability after treatment with C6R8 for 24 hr was analyzed using the WST-1 assay (Fig. 2C). Even in the case when the cells were treated with 100 μM C6R8, cell viability was higher than 90% as compared to the control cells and this was comparable or lower than that of R8. Therefore, modification with hexanoic acid endowed no significant cytotoxicity to R8.

2.2. Internalization methods of C6R8-Alexa

The involvement of endocytosis for the cellular uptake of arginine-rich CPPs has been reported and macropinocytosis is now regarded as one of the major endocytic uptake pathways of these peptides and their conjugates [7,8]. Macropinocytosis is clathrin-independent and actin-driven endocytosis. We have recently demonstrated that the interaction of oligoarginine with membrane-associated proteoglycans induces actin rearrangement and the eventual macropinocytotic uptake of the peptides [10]. To analyze the contribution of macropinocytosis to the cellular uptake of C6R8 as in the case of R8, HeLa cells were treated with 10 μM R8-Alexa or C6R8-Alexa in the presence and absence of 5 μM cytochalasin D (CytD) in α-MEM(+) for 10 min prior to the CLSM observation (Fig. 3A).

In the absence of CytD, C6R8-Alexa yielded significant diffuse signals in the cytosol. There was a range of intensity of the endosome-like C6R8-Alexa signals observed in the cells; some cells yielded intense punctate signals in the perinuclear area together with diffuse cytosolic signals (shown with an arrow) whereas more accumulated signals to the nuclei were observed in other cells (a triangle). On the other hand, R8 yielded only punctate signals and this further confirmed the acceleration effect of the hexanoyl moiety on the translocation of R8-Alexa into the cytosol.

CytD treatment of the cells would lead to F-actin depolymerization and the eventual inhibition of the macropinocytic uptake [18]. Similar to the case of R8-Alexa, a significant decrease in the endosome-like punctate signals of C6R8-Alexa was observed in the CytD-treated cells (Fig. 3A). FACS analysis of the CytD-treated cells showed a 30–40% decrease in the total cellular uptake (Fig. 3B). This suggested the possible involvement of the actin-driven pathways including macropinocytosis in the cellular uptake of C6R8-Alexa. On the other hand, diffuse signals of C6R8-Alexa in the presence of CytD also suggested the contribution of cellular uptake other than the actin-driven pathways.

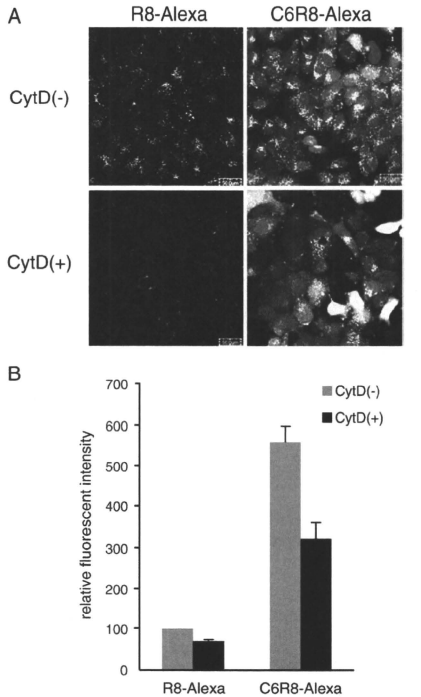

Fig. 3. Effect of cytochalasin D (CytD) on the cellular uptake of C6R8-Alexa. (A) The HeLa cells were incubated with 10 μM C6R8-Alexa or R8-Alexa in the absence and presence of 5 μM CytD for 10 min at 37 °C in α-MEM(+) and distribution of the peptide was analyzed by CLSM. Scale bar, 50 μm. (B) FACS analysis of C6R8-Alexa or R8-Alexa taken up by the cells in 10 min at 37 °C in the absence and presence of 5 μM CytD.

Endocytosis is an energy dependent pathway and is usually suppressed when the cells are treated at 4 °C [19,20]. To assess the involvement of non-endocytic pathways for the internalization of C6R8-Alexa, HeLa cells were incubated with 10 μM R8-Alexa or C6R8-Alexa in α-MEM(+) for 30 min at 37 °C and 4 °C (Fig. 4A). Endosome-like punctate signals were predominantly observed for the cells treated with R8-Alexa at 37 °C and diffuse signals spreading over all the cells together with endosome-like punctate signals for the C6R8-Alexa treated cells (Fig. 4A, upper panels). A significant decrease in the fluorescent intensity was observed when the cells were treated with R8-Alexa or C6R8-Alexa at 4 °C (Fig. 4A, lower panels). However, C6R8-Alexa still yielded significant diffuse signals in the cytosol and nucleus even after this 4 °C-treatment, accompanied by no punctate, endosome-like signals. A similar observation was obtained for the R8-Alexa treated cells at 4 °C, while accompanied by much less intense signals as in the case of the C6R8-Alexa treated cells. These results suggested the possibility that both R8-Alexa and C6R8-Alexa were internalized into cells at 4 °C, presumably by a non-endocytic route and through direct penetration throughout the plasma membranes as reported, [11,19,20]. C6R8-Alexa having an additional hydrophobic affinity to plasma membranes showed a greater extent of translocation through the membranes. It would be interesting to determine why diffuse labeling was only observed for cells treated with these

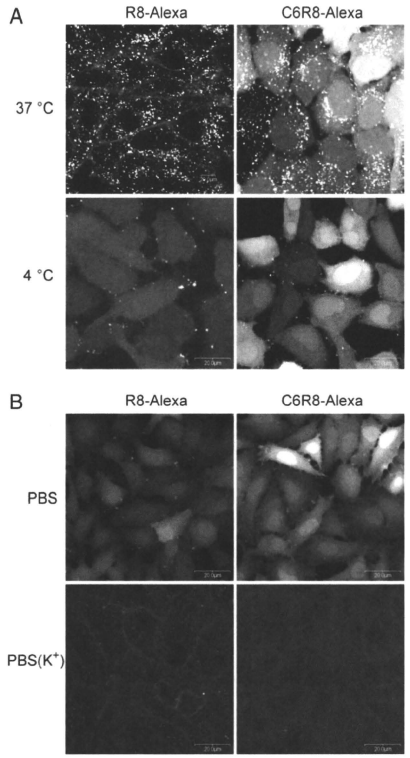

Fig. 4. Effect of low temperature treatment and cancellation of membrane potential on the internalization of C6R8 and R8. (A) The HeLa cells were incubated with 10 μM C6R8-Alexa or R8-Alexa for 30 min at 4 °C or 37 °C in α-MEM(+) and the cellular localization of the peptides was analyzed by CLSM. (B) The HeLa cells were incubated with 5 μM C6R8-Alexa or R8-Alexa for 10 min at 37 °C in PBS(K^+) or PBS. 5 μM peptides were employed to avoid saturation of the fluorescent signals in the CLMS analysis since C6R8-Alexa internalizes into cells more efficiently in PBS than in the α-MEM(+). Scale bar, 20 μm.

peptides at 4 °C. It has been reported that cell-surface accumulation of arginine-rich CPPs at a concentration exceeding a certain threshold leads to direct and energy-independent translocation of the peptides [11,20,21]. Inhibition of endocytic uptake of these peptides at 4 °C would therefore contribute to increase the peptide concentration on plasma membranes and thus promote diffuse cytosolic labeling.

The membrane potential has been suggested as one of the critical factors for cellular uptake of the arginine-rich CPPs [22,23]. We examined whether the translocation of C6R8 is dependent on the membrane potential. Cells were incubated with 5 μM R8-Alexa and C6R8-Alexa for 10 min in PBS(K^+), where Na^+ in the phosphate buffered saline (PBS) is replaced with an equimolar amount of K^+, and this leads to cancellation of the membrane potentials [22]. A drastic decrease in the intracellular fluorescent signals was observed in the CLSM analysis for the cells treated with both R8-Alexa and C6R8-Alexa in PBS(K^+) (Fig. 4B), and this suggested that the membrane potential also plays a crucial role in the translocation of the C6R8-Alexa as in the case of R8-Alexa. Treatment of the cells with R8-Alexa and C6R8-Alexa in PBS (Fig. 4B, upper panels) yielded more diffuse cytosolic labeling than in experiments where the peptide was incubated in α-MEM(+) (Fig. 4A, upper panels). Adsorption of arginine-rich CPPs to serum proteins would reduce cell-surface concentration of the peptides together with cytosolic signals of the peptides as reported previously [11].

2.3. Applicability of C6R8 as a protein/peptide delivery vector

The above results suggested the advantage of C6R8 as an intracellular delivery vector to the R8. Since the effects of cargo molecules on the efficacy of intracellular delivery have been reported, [24,25] we next examined the effect of protein conjugation on the intracellular delivery using C6R8. Conjugates of the Alexa-labeled ubiquitin (9 kDa) with R8 and C6R8 were prepared using the heterobifunctional cross-linking agent EMCS [=*N*-(6-maleimidocaproyloxy)succinimide] (R8-Ub-Alexa and C6R8-Ub-Alexa, respectively) [26]. Treatment of the HeLa cells with 10 μM C6R8-Ub-Alexa at 37 °C for 30 min produced significant punctate signals in the cells (Fig. 5A). Diffuse signals of the conjugates in the cytosol were also observed for ~20% of the cells treated with C6R8-Ub-Alexa. In contrast, only punctate signals with a lower intensity were observed in the R8-Ub-Alexa treated cells. Conjugates of carbonic anhydrase (29 kDa) with these peptides were similarly prepared (R8-CA-Alexa and C6R8-CA-Alexa, respectively) and incubated with HeLa cells. Although C6R8-CA-Alexa produced more intense signals in the cells compared to R8-CA-Alexa, only punctate signals were observed in both cases (Fig. 5B). Therefore, the conjugation with C6R8 also effectively improved the cellular uptake of the proteins. However, as the molecular weight of the cargo molecules was higher, the acceleration effect of the cytosolic translocation seems to become less obvious.

The proapoptotic domain (PAD) peptide has an amphiphilic, cationic sequence of $_D$-(KLAKLAK)$_2$ and is by itself non-toxic to eukaryotic cells even at relatively high concentrations up to 300 μM [27]. However, PAD conjugated to CPPs inhibits cell proliferation in the low micromolar range by perturbation of the mitochondrial membrane and the induction of apoptotic cell death [7]. Here, the effect of the C6R8 conjugation on the efficacy during the intracellular delivery of PAD was assessed in comparison to that by R8 using human malignant glioma cells expressing the wild type p53 protein (A172) and mutant p53 protein (T98G). The PAD was connected with C6R8 or R8 by disulfide cross-linking (C6R8-ss-PAD and R8-ss-PAD, respectively) and treated with these glioma cells (5–20 μM for 24 h), and the viability of the cells was analyzed by the WST-1 assay (Fig. 6A, left). A marked decrease in viability was observed when the A172 cells were treated with C6R8-ss-PAD (10 and 20 μM). At 20 μM, viability of the C6R8-ss-PAD treated cells was less than 20% while that for the R8-ss-PAD treated cells was only 65%. Therefore, C6R8 effectively work as an intracellular delivery vector of the PAD peptide for A172 cells.

On the other hand, different results were obtained using the T98G cells. The treatment of T98G cells with 20 μM C6R8-ss-PAD produced only about a 40% cell death and there was no significant superiority of C6R8 over R8 in this case (Fig. 6A, right). We hypothesized that this would be due to the efficiency in cellular uptake or distribution into the cytosol of the C6R8. Therefore, we examined the total cellular uptake of C6R8-Alexa and R8-Alexa by FACS analysis and CLSM observations in both cells. However, this yielded no significant differences in the cellular uptake of C6R8-Alexa to R8-Alexa between these cells (data not shown). A CLSM analysis of the C6R8-Alexa treated cells showed diffuse cytosolic signals but only punctate signals were obtained for the R8-Alexa treated cells (Fig. 6B). There is currently no distinct explanation at current stage about the

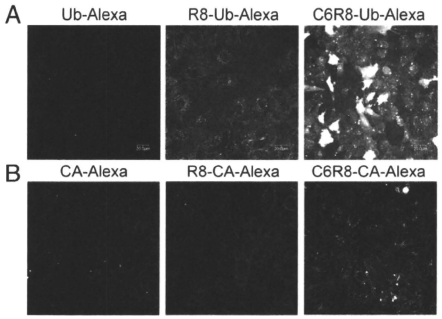

Fig. 5. Intracellular delivery of ubiquitin (Ub) and carbonic anhydrase (CA) using C6R8 and R8. (A) The HeLa cells were treated with C6R8-Ub-Alexa or R8-Ub-Alexa (10 μM) at 37 °C for 30 min in α-MEM(+) prior to the CLSM analysis. Scale bar, 20 μm. (B) The HeLa cells were similarly treated with C6R8-CA-Alexa or R8-CA-Alexa (10 μM) at 37 °C for 30 min.

inconsistency between the extent of cellular uptake (or cytosolic diffusion) and bioactivity of these peptides in T98G cells; the diminished p53 activity of the mutant p53 expressed in the T98G cells may be one possible reason because often it leads to cells with resistance against anti-cancer reagents [28].

3. Conclusion

The results obtained in this study suggest the potential of fatty acid modification of arginine-rich CPPs to improve efficacy in intracellular delivery. We employed R8 as a typical arginine-rich CPP, and the modification with hexanoic acid was shown to produce a considerable improvement in the cellular uptake and cytosolic distribution of the cargo molecules with no significant cytotoxicity. Of note is that all the experiments in this study were conducted using serum-containing medium, and this suggests the potential expandability of this approach for in vivo applications.

C6R8 shares the similarity of internalization methods with R8, including the involvement of macropinocytosis or other actin-driven endocytosis, possible direct translocation into cytosol at 4 °C and contribution of membrane potentials to internalization. Internalization of these peptide vectors and their conjugates with cargos would be accomplished based on a balance of these factors. Lack of a notable cytotoxicity by the C6R8 treatment suggested that the translocation was not accomplished via a simple pore formation or perturbation on the membranes. Detailed analyses of the internalization methods of these peptides referring to the differences in the hydrophobicity may provide novel insights into the modes of peptide–membrane interaction.

Increment of membrane interaction by hexanoic acid modification led to a higher extent of cytosolic distribution of C6R8 as compared to R8. Acylation of R8 with decanoic or the longer-chain fatty acids produced a higher cytotoxicity and accompanied the aggregate formation. Therefore, there must be a range of hydrophobicity to accomplish the optimum cytosolic delivery. Recently, we reported that the addition of a hydrophobic peptide segment [FFLIPKG, designated as penetration accelerating sequence (Pas)] to arginine-rich CPPs also facilitated the cytosolic distribution of the cargo molecules [29]. Therefore, adding the hydrophobic cores to arginine-rich CPPs could be a way to improve their efficiency of the cytosolic delivery. On the other hand, we also found that there can be a certain differences in the internalization efficiency among the peptides with a similar hydrophobicity [e.g., Pas modified R8 (FFLIPKG-RRRRRRRR) and the retro peptide RRRRRRRR-GKPILFF] and it should be noted that there must be other additional factors that determine the methods of internalization of these peptides.

When the C6R8 was conjugated with ubiquitin (9 kDa), C6R8-Ub-Alexa showed a significantly higher cellular uptake and cytosolic distribution into the cytosol than R8-Ub-Alexa. However, for the delivery of carbonic anhydrase (28 kDa), the effect of acylation became smaller, presumably due to larger molecular size of the carbonic anhydrase that prevents penetration through the membranes. Although further evaluation is necessary, this study has provided important information on the design of peptide-based intracellular delivery vectors.

4. Experimental procedures

4.1. Peptides

For the preparation of the N-terminus acylated peptides, the peptide chain was constructed using Fmoc (9-fluorenylmethyloxycarbonyl) solid-phase peptide synthesis, and the N-terminus of the peptide resin was acylated using the corresponding fatty acid with diisopropylcarbodiimide in the presence of N-hydroxybenzotriazole as coupling agents as previously reported [12]. Treatment of the acylated peptide resin with trifluoroacetic acid in the presence of 5% ethanedithiol followed by reverse phase high-performance liquid chromatography (RP-HPLC) produced the desired peptides. For Alexa labeling, the HPLC purified CnR8GC peptides ($n=4$, 6, 10, 14, and 18) were treated with the Alexa Fluor 488 C_5 maleimide sodium salt (Invitrogen) as previously reported [10]. Actual sequences of the peptides follows: C6R8, C_5H_{11}CO-RRRRRRRR-amide; CnR8GC, C_mH_{2m+1}CO-RRRRRRRRGC-amide ($n=4$, 6, 10, 14, and 18; $m=n-1$); CnR8-Alexa, C_mH_{2m+1}CO-RRRRRRRRGC(Alexa488)-amide ($n=4$, 6, 10, 14, and 18; $m=n-1$); R8, RRRRRRRR-amide; R8GC, RRRRRRRRGC-amide; and R8-Alexa, RRRRRRRRGC(Alexa488)-amide.

The C6R8-ss-PAD was prepared via selective disulfide cross-linking between C6R8GC and the CG-$_D$-(KLAKLAK)$_2$-amide by activation of the cysteine in the CG-$_D$-(KLAKLAK)$_2$-amide via pyridine sulfenylation [7]. For the preparation of R8-ss-PAD, R8GC was employed instead of C6R8GC.

The purity and structures of the peptides used in this study were confirmed by HPLC and matrix-assisted laser desorption ionization-time-of-flight mass spectrometry (MALDI-TOFMS), respectively.

4.2. Conjugates of ubiquitin with R8 and C6R8

Alexa 488-labeling of ubiquitin was conducted by the treatment of ubiquitin with Alexa 488 carboxylic acid, succinimidyl ester (Invitrogen) (3 eq) followed by cross-linking with R8GC or C6R8GC using *N*-(6-maleimidocaproyloxy)succinimide (EMCS) (Dojindo) [3 eq each to Alexa-labeled ubiquitin] as reported [26]. After the reactions, the excess reagents or peptides were removed by ultrafiltration using a Microcon YM-10 centrifuging filter (Millipore) (molecular weight cut off = 10,000) at 14,000×*g* for 24 min. Ubiquitin was obtained from Sigma. Conjugates of carbonic anhydrase (Sigma) with R8GC or C6R8GC were similarly prepared (MicroconYM-30 was used for ultrafiltration). The concentration of these conjugates was described in this report on the basis of the absorbance of fluorophore.

4.3. Cell culture

Human cervical cancer-derived HeLa cells were cultured on 100 mm dishes in α-minimum essential medium supplemented with 10% (v/v) fetal bovine serum (GIBCO) [α-MEM(+)]. Human glioblastoma-derived cells including A172 (wild type) and T98G (variant) were cultured in D-MEM (Dulbecco's Modified Eagle Medium) supplemented with 10% (v/v) fetal bovine serum (GIBCO).

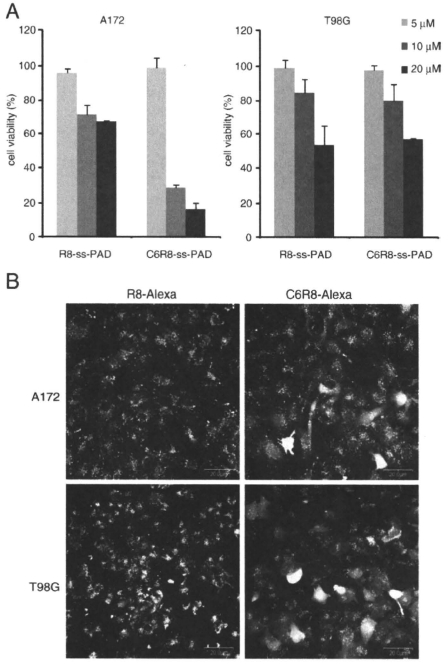

Fig. 6. Assessment of internalization efficiency in terms of bioactivity exerted by the intracellularly delivered PAD peptide. (A) C6R8-ss-PAD and R8-ss-PAD were incubated with A172 and T98G cells for 24 h and the cell viability was analyzed by the WST-1 assay. (B) The CLSM analysis of the A172 and T98G cells treated with C6R8-Alexa and R8-Alexa (10 μM) for 30 min.

Cells were maintained at 37 °C in a humidified 5% CO_2 incubator, and a subculture was performed every 3–4 days.

4.4. Confocal microscopy

HeLa cells (1.5×10^5 cells/well) were plated in 35 mm glass-bottomed dishes (Iwaki) and cultured for 48 h. The cells were washed twice with serum-free medium prior to incubation with the peptides or proteins in 200 μL of α-MEM containing 10% (v/v) fetal bovine serum [α-MEM (+)]. After incubation for 30 min, the incubated medium was removed and the cells were washed twice with cold serum-free medium. The intracellular distribution was immediately analyzed without fixing using a confocal laser scanning microscope (Olympus FV300) equipped with a ×40 objective. For experiments using cytocharasin D (CytD), the cells were preincubated with 5 μM CytD in α-MEM (+) for 30 min prior to incubation with the peptide and CytD in α-MEM (+) for 10 min. For the 4 °C experiments, cells were preincubated in a refrigerator (4 °C) for 1 h. Washing and incubation of the cells were then conducted using cold medium and the 4 °C refrigerator, respectively, prior to observation of the cells. For experiments investigating the contribution of the membrane potential, a buffer PBS(K^+) in which the sodium salts in PBS(−) were replaced with equimolar amounts of the equivalent potassium salts was used.

4.5. Flow cytometry

HeLa cells (4×10^4 cells/well) were plated in 24 well microplates (Iwaki) and cultured for 48 h. The cells were washed twice with serum-free medium prior to incubation with peptides (10 μM) in α-MEM (+). The cells were then washed twice with PBS containing 0.5 mg/mL heparin to ensure the removal of cell-surface adsorbed peptides and incubated with 0.01% trypsin in PBS for 10 min at 37 °C. The cells were harvested and centrifuged at 3000 rpm for 5 min. The cell pellet was then suspended with PBS containing 0.5 mg/mL heparin followed by centrifuging. After an additional two washes with PBS and centrifuging, the cells were suspended in 400 μL of PBS and filtered for fluorescence analysis by a FACS Calibur flow cytometer (BD Biosciences) using a 488 nm laser excitation and a 515–545 nm emission filter. Each sample was analyzed for 10,000 events.

4.6. WST-1 assay

HeLa, A172, and T98G cells (5×10^3 cells/well) were plated in 96 well microplates (Iwaki) and cultured for 48 h. After removing the medium, the cells were incubated with peptide-containing medium for 24 h at 37 °C and then a WST-1 assay were conducted following the procedures provided by the supplier (Roche).

Acknowledgments

This work was supported in part by Grants-in-Aid for Scientific Research from the Ministry of Education, Culture, Sports, Science and Technology of Japan. H. H. and K. T. are grateful for a JSPS Research Fellowship for Young Scientists.

References

[1] A. El-Sayed, S. Futaki, H. Harashima, Delivery of macromolecules using arginine-rich cell-penetrating peptides: ways to overcome endosomal entrapment, AAPS J. 11 (2009) 13–22.
[2] S. Futaki, Oligoarginine vectors for intracellular delivery: design and cellular-uptake mechanisms, Biopolymers 84 (2006) 241–249.
[3] J.S. Wadia, S.F. Dowdy, Transmembrane delivery of protein and peptide drugs by TAT-mediated transduction in the treatment of cancer, Adv. Drug Deliv. Rev. 57 (2005) 579–596.
[4] E.A. Goun, T.H. Pillow, L.R. Jones, J.B. Rothbard, P.A. Wender, Molecular transporters: synthesis of oligoguanidinium transporters and their application to drug delivery and real-time imaging, Chembiochemistry 7 (2006) 1497–1515.
[5] S. Futaki, T. Suzuki, W. Ohashi, T. Yagami, S. Tanaka, K. Ueda, Y. Sugiura, Arginine-rich peptides. An abundant source of membrane-permeable peptides having potential as carriers for intracellular protein delivery, J. Biol. Chem. 276 (2001) 5836–5840.
[6] J.P. Richard, K. Melikov, E. Vives, C. Ramos, B. Verbeure, M.J. Gait, L.V. Chernomordik, B. Lebleu, Cell-penetrating peptides. A reevaluation of the mechanism of cellular uptake, J. Biol. Chem. 278 (2003) 585–590.
[7] I. Nakase, M. Niwa, T. Takeuchi, K. Sonomura, N. Kawabata, Y. Koike, M. Takehashi, S. Tanaka, K. Ueda, J.C. Simpson, A.T. Jones, Y. Sugiura, S. Futaki, Cellular uptake of arginine-rich peptides: roles for macropinocytosis and actin rearrangement, Mol. Ther. 10 (2004) 1011–1022.
[8] J.S. Wadia, R.V. Stan, S.F. Dowdy, Transducible TAT-HA fusogenic peptide enhances escape of TAT-fusion proteins after lipid raft macropinocytosis, Nat. Med. 10 (2004) 310–315.
[9] I. Nakase, T. Takeuchi, G. Tanaka, S. Futaki, Methodological and cellular aspects that govern the internalization mechanisms of arginine-rich cell-penetrating peptides, Adv. Drug Deliv. Rev. 60 (2008) 598–607.
[10] I. Nakase, A. Tadokoro, N. Kawabata, T. Takeuchi, H. Katoh, K. Hiramoto, M. Negishi, M. Nomizu, Y. Sugiura, S. Futaki, Interaction of arginine-rich peptides with membrane-associated proteoglycans is crucial for induction of actin organization and macropinocytosis, Biochemistry 46 (2007) 492–501.
[11] M. Kosuge, T. Takeuchi, I. Nakase, A.T. Jones, S. Futaki, Cellular internalization and distribution of arginine-rich peptides as a function of extracellular peptide concentration, serum, and plasma membrane associated proteoglycans, Bioconjug. Chem. 19 (2008) 656–664.
[12] S. Futaki, W. Ohashi, T. Suzuki, M. Niwa, S. Tanaka, K. Ueda, H. Harashima, Y. Sugiura, Stearylated arginine-rich peptides: a new class of transfection systems, Bioconjug. Chem. 12 (2001) 1005–1011.

[13] L. Tönges, P. Lingor, R. Egle, G.P. Dietz, A. Fahr, M. Bähr, Stearylated octaarginine and artificial virus-like particles for transfection of siRNA into primary rat neurons, RNA 12 (2006) 1431–1438.
[14] W.J. Kim, L.V. Christensen, S. Jo, J.W. Yockman, J.H. Jeong, Y.H. Kim, S.W. Kim, Cholesteryl oligoarginine delivering vascular endothelial growth factor siRNA effectively inhibits tumor growth in colon adenocarcinoma, Mol. Ther. 14 (2006) 343–350.
[15] U. Koppelhus, T. Shiraishi, V. Zachar, S. Pankratova, P.E. Nielsen, Improved cellular activity of antisense peptide nucleic acids by conjugation to a cationic peptide-lipid (CatLip) domain, Bioconjug. Chem. 19 (2008) 1526–1534.
[16] A.R. Nelson, L. Borland, N.L. Allbritton, C.E. Sims, Myristoyl-based transport of peptides into living cells, Biochemistry 46 (2007) 14771–14781.
[17] J. Fernandez-Carneado, M.J. Kogan, N. Van Mau, S. Pujals, C. Lopez-Iglesias, F. Heitz, E. Giralt, Fatty acyl moieties: improving Pro-rich peptide uptake inside HeLa cells, J. Pept. Res. 65 (2005) 580–590.
[18] P. Sampath, T.D. Pollard, Effects of cytochalasin, phalloidin, and pH on the elongation of actin filaments, Biochemistry 30 (1991) 1973–1980.
[19] M.M. Fretz, N.A. Penning, S. Al-Taei, S. Futaki, T. Takeuchi, I. Nakase, G. Storm, A.T. Jones, Temperature-, concentration- and cholesterol-dependent translocation of L- and D-octa-arginine across the plasma and nuclear membrane of CD34$^+$ leukaemia cells, Biochem. J. 403 (2007) 335–342.
[20] C.L. Watkins, D. Schmaljohann, S. Futaki, A.T. Jones, Low concentration thresholds of plasma membranes for rapid energy-independent translocation of a cell-penetrating peptide, Biochem. J. 420 (2009) 179–189.
[21] F. Duchardt, M. Fotin-Mleczek, H. Schwarz, R. Fischer, R. Brock, A comprehensive model for the cellular uptake of cationic cell-penetrating peptides, Traffic 8 (2007) 848–866.
[22] J.B. Rothbard, T.C. Jessop, R.S. Lewis, B.A. Murray, P.A. Wender, Role of membrane potential and hydrogen bonding in the mechanism of translocation of guanidinium-rich peptides into cells, J. Am. Chem. Soc. 126 (2004) 9506–9507.
[23] T. Takeuchi, M. Kosuge, A. Tadokoro, Y. Sugiura, M. Nishi, M. Kawata, N. Sakai, S. Matile, S. Futaki, Direct and rapid cytosolic delivery using cell-penetrating peptides mediated by pyrenebutyrate, ACS Chem. Biol. 1 (2006) 299–303.
[24] J.R. Maiolo, M. Ferrer, E.A. Ottinger, Effects of cargo molecules on the cellular uptake of arginine-rich cell-penetrating peptides, Biochim. Biophys. Acta 1712 (2005) 161–172.
[25] G. Tünnemann, R.M. Martin, S. Haupt, C. Patsch, F. Edenhofer, M.C. Cardoso, Cargo-dependent mode of uptake and bioavailability of TAT-containing proteins and peptides in living cells, FASEB J. 20 (2006) 1775–1784.
[26] K. Takayama, A. Tadokoro, S. Pujals, I. Nakase, E. Giralt, S. Futaki, Novel system to achieve one-pot modification of cargo molecules with oligoarginine vectors for intracellular delivery, Bioconjug. Chem. 20 (2009) 249–257.
[27] H.M. Ellerby, W. Arap, L.M. Ellerby, R. Kain, R. Andrusiak, G.D. Rio, S. Krajewski, C.R. Lombardo, R. Rao, E. Ruoslahti, D.E. Bredesen, R. Pasqualini, Anti-cancer activity of targeted pro-apoptotic peptides, Nat. Med. 5 (1999) 1032–1038.
[28] S. Fan, W.S. El-Deiry, I. Bae, J. Freeman, D. Jondle, K. Bhatia, A.J. Fornace Jr., I. Magrath, K.W. Kohn, P.M. O'Connor, p53 gene mutations are associated with decreased sensitivity of human lymphoma cells to DNA damaging agents, Cancer Res. 54 (1994) 5824–5830.
[29] K. Takayama, I. Nakase, H. Michiue, T. Takeuchi, K. Tomizawa, H. Matsui, S. Futaki, Enhanced intracellular delivery using arginine-rich peptides by the addition of penetration accelerating sequences (Pas), J. Control. Release 138 (2009) 128–133.

Journal of Controlled Release 143 (2010) 311–317

Contents lists available at ScienceDirect

Journal of Controlled Release

journal homepage: www.elsevier.com/locate/jconrel

Nanoparticles for *ex vivo* siRNA delivery to dendritic cells for cancer vaccines: Programmed endosomal escape and dissociation☆

Hidetaka Akita [a], Kentaro Kogure [a,1], Rumiko Moriguchi [a], Yoshio Nakamura [a], Tomoko Higashi [a], Takashi Nakamura [a], Satoshi Serada [b], Minoru Fujimoto [b], Tetsuji Naka [b], Shiroh Futaki [c], Hideyoshi Harashima [a,*]

[a] Faculty of Pharmaceutical Sciences, Hokkaido University, Kita-12, Nishi-6, Kita-ku, Sapporo, Hokkaido 060-0812, Japan
[b] Laboratory for Immune Signal, National Institute of Biomedical Innovation, 7-6-8 Saito-Asagi, Ibaraki, Osaka 567-0085, Japan
[c] Institute for Chemical Research, Kyoto University, Uji, Kyoto 611-0011, Japan

ARTICLE INFO

Article history:
Received 14 September 2009
Accepted 7 January 2010
Available online 15 January 2010

Keywords:
siRNA
Vaccination
Dendritic cells
SOCS1
Intracellular trafficking

ABSTRACT

We previously developed octaarginine (R8)-modified lipid envelope-type nanoparticles for siRNA delivery (R8-MEND). Herein, we report on their *ex vivo* siRNA delivery to primary mouse bone marrow-derived dendritic cells (BMDCs) for potential use as a cancer vaccine. Quantitative imaging analysis of the intracellular trafficking of siRNA revealed that the dissociation process, as well as the rate of endosomal escape limits the siRNA efficiency of the prototype R8-MEND, prepared by the hydration method (R8-$MEND_{hydo}$). Successful endosomal escape was achieved by using a pH-dependent fusogenic peptide (GALA) modified on a lipid mixture that was optimized for endosomal fusion. Furthermore, a modified protocol for the preparation of nanoparticles, mixing the siRNA/STR-R8 complex and small unilamellar vesicles (R8/GALA-$MEND_{SUV}$), results in a more homogenous, smaller particle size, and results in a more efficient intracellular dissociation. Gene knockdown of the suppressor of cytokine signaling 1 (SOCS1), a negative-feedback regulator of the immune response in BMDCs resulted in an enhanced phosphorylation of STAT1, and the production of proinflammatory cytokines. Moreover, SOCS1-silenced BMDCs were more potent in suppressing tumor growth. Collectively, these results show that siRNA loaded in R8/GALA-$MEND_{SUV}$ efficiently suppresses endogenous gene expression and consequently enhances dendritic cell-based vaccine potency *in vivo*.

1. Introduction

RNA interference (RNAi) was discovered [1,2], in the latter part of the 20th century. This discovery represents a promising technique for use in the functional analysis of endogenous genes, and for curing intractable genetic diseases by the sequence-specific cleavage of mRNA [3–5]. One of the highly potential applications for the clinical use of siRNA is cancer vaccination. The suppressor of cytokine signaling 1 (SOCS1) is a negative-feedback regulator of immune cell responses to cytokines. Its expression is induced by cytokine-mediated stimulation, and is responsible for the negative-feedback of immunoresponse by blocking Janus kinase (JAK)-signal transducers, and activators of transcription (STAT) signaling pathways [6]. The suppression of SOCS1 gene expression in dendritic cells using a lentiviral vector has been shown to enhance their immunostimulatory capacity and to result in an enhanced antiviral and antitumor response [7,8]. However, the use of a viral vector may have unexpected, and serious adverse effects such as excessive inflammation [9] and oncogenicity due to the random insertion of viral genomic DNA into chromosomal DNA [10]. Therefore, non-viral delivery vehicles, which satisfy requirements for both high efficiency and safety, are essential for the realization of clinical applications of siRNA [11]. To be recognized by a RNA-induced silencing complex (RISC), siRNA must be delivered to the cytoplasm via invasion of the membrane. Therefore, novel nanotechnology is essential if various functional devices are integrated into one nano carrier for achieving both active cellular entry and endosomal escape. For an in vivo application via systemic administration, the loading of siRNA into the liposomal particle is one of the more desirable strategies for conferring stability in the systemic circulation, and the efficient delivery of the siRNA to a target organ (i.e. liver and tumor) [12–15].

We recently proposed a packaging concept referred to as "Programmed Packaging" [16,17], in which various types of devices are incorporated into nanoparticles in a manner such that their topology is controlled. Based on this concept, multifunctional envelope-type

☆ Hidetaka Akita, Kentaro Kogure and Rumiko Moriguchi equally contributed to this study. These authors are listed alphabetically in accordance with family name.

* Corresponding author. Laboratory for Molecular Design of Pharmaceutics, Faculty of Pharmaceutical Sciences, Hokkaido University, Kita-12, Nishi-6, Kita-ku, Sapporo, Hokkaido 060-0812, Japan. Tel.: +81 11 706 3919; fax: +81 11 706 4879.
E-mail address: harasima@pharm.hokudai.ac.jp (H. Harashima).
[1] Present address: "Kyoto Pharmaceutical University, 5 Nakauchi-cho, Misasagi, Yamashina-ku, Kyoto 607-8414, Japan".

0168-3659/$ – see front matter © 2010 Elsevier B.V. All rights reserved.
doi:10.1016/j.jconrel.2010.01.012

nano-devices (MEND) were originally established for use as a plasmid DNA (pDNA) carrier. For the application of this system to siRNA delivery, nano-sized complexed cores were similarly formed with siRNA using an amphiphatic polycation (i.e. stearylated octaarginine; STR-R8), which leads to its loading in the lipid envelope by hydration methods ($MEND_{hydo}$) [18]. The outer surface of the $MEND_{hydo}$ can be modified with octaarginine (R8), which induces cellular uptake of the particle by macropinocytosis, a useful pathway that avoids lysosomal degradation.

In the present study, we report on a mechanism-based development of a siRNA delivery system, which can knockdown the gene expression at 1/10 the dose. For this purpose, a pH-sensitive fusogenic peptide was modified for endosomal escape. Furthermore, the packaging method was altered, resulting in the formation of a more homogenous and smaller particle, which is advantageous in terms of improving the intracellular dissociation process. In this development process, we made maximum use of the quantitative imaging analysis for the intracellular trafficking of siRNA (confocal image-assisted 3-dimensionally integrated quantification; CIDIQ), which provides information on the rate-limiting process of the siRNA carriers. Finally we successfully demonstrate *ex vivo* siRNA delivery to primary mouse bone marrow-derived dendritic cells (BMDCs) for potential use as a cancer vaccine.

2. Materials and methods

2.1. Materials and cell lines

1,2-Dioleoyl-*sn*-glycero-3-phosphoethanolamine (DOPE) and 4-nitrobenzo-2-oxa-1,3-diazolyl-DOPE (NBD-DOPE) were purchased from AVANTI Polar Lipids Inc. (Alabaster, AL). Cholesteryl hemisuccinate (5-Cholesten-3β-ol 3-hemisuccinate; CHEMS), ovalbumin (OVA) and lipopolysaccharide (LPS) were obtained from Sigma-Aldrich Co. (St. Louis, MO). Cholesteryl GALA (Chol-GALA) was custom-synthesized by KURABO, as reported previously [19]. Lipofectamine 2000 was obtained from Invitrogen Co. (Carlsbad, CA). The $OVA_{257-264}$ peptide (SIINFEKL) was synthesized by Kurabo Industries (Osaka, Japan). HeLa cells and E.G.7-OVA cells were purchased from RIKEN BioResource Center (Ibaraki, Japan) and the American Type Culture Collection (Manassas, VA), respectively. siRNA sequences used in the present study, and establishment of HeLa cells stably expressing luciferase (HeLa-GL3) were described in Supplemental Information.

2.2. Animals

Female C57BL/6J mice (6–8-weeks old) were obtained from CLEA Japan Inc. (Tokyo, Japan) and maintained under specific pathogen-free conditions. The use of the mice was approved by the Pharmaceutical Science Animal Committee of Hokkaido University.

2.3. siRNA-loading MENDs

The prototype R8-MEND was prepared by the hydration method (R8-$MEND_{hydo}$) as described previously [18]. The MEND prepared with another protocol (R8-$MEND_{SUV}$) was prepared by mixing small unilamellar vesicles (SUVs) with a suspension of siRNA/STR-R8. For the preparation of the SUV, lipid films containing DOPE and phosphatidic acid (PA) at a ratio of 7:2 (total lipid content: 0.55 μmol) were hydrated with 1 ml of 10 mM HEPES buffer (pH 7.4) for 10 min at room temperature. For modification of $MEND_{SUV}$ with GALA, 1 mol% of Chol-GALA was added in the lipid composition. The hydrated lipid film was then sonicated using a probe-type sonicator, and the siRNA/STR-R8 complex (33 μg siRNA/ml) was then mixed with the SUVs at a ratio of 1:2 (v/v). Finally, surfaces of $MEND_{SUV}$ were modified by adding a STR-R8 solution (10 mol% of total lipids), followed by incubation for 30 min. Gene knockdown activity of MENDs are evaluated as described in Supplemental Information.

2.4. CIDIQ analysis

The efficiencies of endosomal escape and dissociation were assessed by confocal image-based quantification as described in a recent report [20,21]. For the evaluation of endosomal escape, MENDs prepared with Alexa546-labeled siRNA was transfected to HeLa-GL3 cells. At 2.5 h after transfection, the endosomes/lysosomes were stained with Lysotracker green to discriminate between siRNA in the endosomes/lysosomes and the cytosol.

For analysis of the dissociation of the siRNA from MENDs, they were prepared with Alexa546-labeled siRNA and an NBD-labeled lipid layer. For labeling the lipid envelope with NBD, 1% of NBD-DOPE was incorporated into the lipid composition. Confocal images were captured at 9 h post-transfection, and thereafter quantitatively analyzed. Detail method for the quantitative analysis is described in Supplemental information.

2.5. Quantification of cellular uptake of MENDs by flow cytometry

The cellular uptake of the MENDs was assessed by flow cytometry. MENDs loading the Alexa546-labeled siRNA were prepared as described above. For the quantification of cellular uptake, HeLa-GL3 cells were seeded at a density of 5.0×10^4 cells per 6-well plate in the growth medium. After 24 h, the cells were incubated with the MENDs (71 nM of Alexa546-labeled siRNA) in serum-free medium for 1 h. The cells were washed once with PBS supplemented with 0.5% bovine serum albumin and 0.1% NaN_3, and then trypsinized and collected in a microtube, followed by washing two additional times by repeated precipitation of the cells by centrifugation (1500 rpm, 4 °C, 5 min) and resuspended in 1 ml of PBS including heparin (20 U/ml). Finally, the cells were suspended in 1 ml of PBS. The cell suspension was then filtered through nylon mesh to remove cell aggregates and dust, and the cells were then analyzed by flow cytometry (FACScan, Becton Dickinson).

2.6. Preparation of BMDCs of mice

BMDCs were prepared as reported previously [22] with minor modifications. Briefly, bone marrow cells were cultured for 4 h in RPMI1640 medium containing 50 μmol/l 2-mercaptoethanol, 10 mM HEPES, 1 mM sodium pyruvate, 100 U/ml penicillin–streptomycin, and 10% fetal calf serum. Non-adherent cells were harvested and cultured in the same medium supplemented with 10 ng/ml GM-CSF (R&D Systems, Basel, Switzerland). On days 2 and 4, non-adherent cells were removed, and adherent cells were cultured in fresh medium containing 10 ng/ml GM-CSF. On day 6, non-adherent and loosely adherent cells were used as immature DCs. Cell surface expression of CD11c in more than 85% of the cell population was confirmed by flow activated cell sorting (FACS) analysis.

2.7. Evaluation of gene knockdown activity of MENDs in BMDCs

To evaluate the silencing effect against GAPDH, BMDCs (1.2×10^6 cells) were incubated with R8/GALA-$MEND_{SUV}$ loading 60 pmol siRNA for 2 h at 37 °C in 0.5 ml of serum-free OPTI-MEM I containing 10 ng/ml GM-CSF in 12-well plate. Then, 1 ml of RPMI1640 medium containing GM-CSF was added to the cells, and incubated further 22-h incubation.

In the case of SOCS1 knockdown, BMDCs were transfected with R8/GALA-$MEND_{SUV}$ containing 40 pmol siRNA for 2 h. RPMI1640 medium containing GM-CSF was then added to the cells, followed by further 2-h incubation. BMDCs were washed and incubated in the fresh medium for 2 h at 37 °C and then stimulated with IFN-γ (50 ng/ml) for 24 h. SOCS1 expression in BMDCs is evaluated as described in Supplemental Information.

2.8. Quantification of cytokine production from BMDCs

Non-treated or siRNA-transfected BMDCs were stimulated with IFN-γ (50 ng/ml) for 24 h. Concentrations of TNF-α and IL-6 in the culture supernatants were measured by Quantikine (R&D Systems).

2.9. DC immunization and tumor challenge

Immature BMDCs transfected with control siRNA or anti-SOCS1 siRNA were pulsed with OVA peptides (0.5 μM) and OVA protein (50 μg/ml) at 37 °C for 30 min, followed by stimulation with LPS (0.5 μg/ml) for 1 h to develop mature BMDCs. Then, 3.8×10^5 cells were washed with PBS to remove extracellular LPS, and injected into the hind footpads of C57BL/6 mice. One week after immunization, 8×10^5 E.G.7-OVA cells were inoculated subcutaneously into the right flank of immunized mice. Tumor volume was calculated by the following formula: (major axis × minor axis^2) × 0.52.

3. Results

3.1. Gene knockdown activity of MENDs

We wish to report herein on a siRNA delivery system that is effective at low dose, and its development processes with the aid information concerning intracellular trafficking. The carrier was applied to the *ex vivo* gene knockdown of SOCS1 in BMDCs to enhance the effect of a cancer vaccination. Since the siRNAs are incorporated into Argonaute 2 (AGO2) and the RNAi-induced silencing complex (RISC) is in the cytosol, the disposition of siRNA in the cytoplasmic region strongly reflects the efficiency of siRNA. BMDC is not appropriate for the imaging analysis of intracellular trafficking of siRNA, since the volume of the cytoplasmic region is small. Therefore, we first improved the carriers using HeLa-GL3 cells.

In initial experiments, the gene knockdown activity of prototype R8-MEND prepared with hydration method (R8-MEND$_{hydo}$) was evaluated (Fig. 1a). The R8-MEND$_{hydo}$ was found to have a strong gene knockdown effect (>75%) against a HeLa-GL3 at a concentration of approximately 120 nM. However, when the dose was decreased, the gene knockdown effect gradually decreased, with an IC_{50} of approximately 75 nM, and eventually decreased to >10% at 1/10 of the original dose. To achieve a promising breakthrough, the gene knockdown efficiency per 1 particle of siRNA carrier must be substantially improved in order to achieve minimum clinical dosing to avoid any undesirable side effects.

To clearly show the stepwise upgrading of MENDs, the knockdown efficiencies of MENDs in final form (R8/GALA-MEND$_{SUV}$; red bar), and in intermediate forms (blue and yellow bars) at low dose (12 nM) are summarized in Fig. 1b. Improving cytoplasmic delivery, endosome-fusion and/or disruption efficiency are commonly employed tactics. One such membrane-fusion inducer is GALA [23–25], a pH-dependent fusogenic peptide, which induces loaded cargos to be released into the cytosol [19,26]. For the surface display of GALA in a lipid envelope, Chol-GALA was then incorporated at 1 mol% of total lipid [19]. In addition, we recently demonstrated that R8-modified liposomes composed of DOPE/PA = 7/2 are capable of enhancing the cytoplasmic delivery of macromolecules derived from its highly fusogenic activity to endosomes [27,28].

In the light of these previous achievements, R8-MENDs were prepared with a lipid composition of DOPE/PA = 7/2 plus 1% Chol-GALA (R8/GALA-MEND$_{hydo}$). Gene knockdown activity was evaluated at 1/10 of the dose (12 nM), where the gene knockdown effect was negligible in the case of a conventional R8-MEND$_{hydo}$ composed of DOPE/CHEMS (Fig. 1b; black bar). However, regardless of these modification, gene knockdown activity continued to be marginal (approximately 15%, Fig. 1b; blue bar).

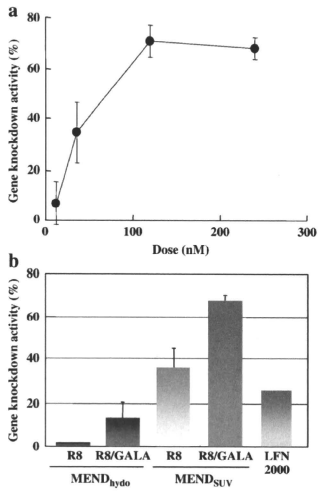

Fig. 1. Gene knockdown activity of MENDs. Function of R8- and R8/GALA-MENDs prepared with hydration method and SUV-mixing method. a. Dose-dependent knockdown effect of the luciferase gene by a prototype R8-MEND$_{hydo}$. MENDs loading siRNA against GFP or luciferase were incubated with HeLa-GL3. Gene knockdown activity was calculated as the percentage of decrease in luciferase activity in the anti-luciferase siRNA treatment to that for the anti-GFP siRNA treatment. b. Silencing effect of MEND$_{hydo}$ and MEND$_{SUV}$ loading anti-luciferase siRNA on luciferase activity of HeLa-GL3. siRNA-loading MENDs with or without GALA modification were added to HeLa-GL3 cells at 12 nM siRNA for 24 h. Luciferase activities were measured as described in Methods. Data are represented as the mean ± SD.

Here, we wish to report that siRNA activity can be dramatically improved by modifying the method used to prepare the MEND (R8/GALA-MEND$_{SUV}$). The positively charged siRNA/STR-R8 complexed core is incubated with negatively charged small unilamellar vesicles (SUVs) composed of DOPE/PA = 7:2 plus 1 mol% of Chol-GALA. The surface of the resulting particles is then modified with STR-R8. As a result, the R8/GALA-MEND$_{SUV}$ particles are smaller in size, compared to the R8/GALA-MEND$_{hydo}$. Furthermore, the polydispersity index of the MEND$_{SUV}$ preparation is smaller, suggesting that the sizes of the prepared MENDs are more uniform (Table 1). The most significant finding is that the knockdown effect was dramatically increased to more than 70% (Fig. 1b, red bar) even at 1/10 the dose, indicating that the knockdown efficiency per 1 particle of siRNA was successfully improved by 10 times. When the GALA modification was not employed (R8-MEND$_{SUV}$), the knock down activity was reduced to 40% (Fig. 1b, yellow), suggesting that GALA modification of the MEND$_{SUV}$ is a valid strategy for the efficient cytoplasmic delivery of siRNA. At this dosage, LFN2000 showed only a slight gene knockdown

Table 1
Physicochemical characteristics of MENDs.

	R8-MEND$_{hydo}$	R8/GALA-MEND$_{hydo}$	R8/GALA-MEND$_{SUV}$
Size (nm)	172.8	178	131.5
Z-potential (mV)	52.5	47.4	42.6
PDI	0.25	0.26	0.17

effect (Fig. 1b, green), suggesting that the R8/GALA-MEND$_{SUV}$ is a highly efficient gene knockdown system. The key to the success of this strategy can be attributed to the quantitative analysis of the intracellular trafficking of siRNA as described in the following sections.

3.2. Evaluation of endosomal escape efficiency

In the present study, the intracellular trafficking of MENDs was evaluated by means of confocal image-assisted 3-dimensionally integrated quantification (CIDIQ; Fig. 2a) [20,21]. Cells were transfected with R8-MEND$_{hydo}$ loading Alaxa543-labeled siRNA, and the endosome/lysosome fraction was then stained with Lysotracker Green at 2.5 h post-transfection. Z-series of images were then captured by confocal laser scanning microscopy (Fig. 2b and c for R8-MEND$_{hydo}$ and R8/GALA-MEND$_{hydo}$, respectively). As a result, siRNA were detected as clustered forms, as shown in Fig. 2b. The siRNA signals colocalized with Lysotracker Green (yellow clusters) are denoted as siRNAs in endosomes/lysosomes. In addition, the siRNAs signals that are not colocalized with Lysotracker Green (red clusters) are denoted as those that escaped from endosome/lysosomes. For quantification, the pixel areas of the siRNA clusters detected in the cytosol (red clusters) and in endosomes/lysosomes (yellow clusters) were separately integrated through all of the Z-series of images (S (red) and S(yellow), respectively). Endosomal escape efficiency was denoted as S(red) divided by the total of S(red) and S(yellow). The calculated endosomal escape efficiency of R8-MEND$_{hydo}$ in 15 individual cells indicated that an average endosomal escape efficiency of 52.4% (Fig. 2d). In contrast, siRNA were observed to be predominant in the cytosol in some cells (Fig. 2c) in R8/GALA-MEND$_{hydo}$. Quantitative evaluation showed that the endosome escape efficiency was increased to an average of approximately 70% (Fig. 2d). The enhanced endosomal escape efficiency may be responsible for the slight improvement in gene knockdown activity (Fig. 1d; blue bar). However, the discrepancy between the slight gene knockdown effect and the high (approx.70%) endosomal escape efficiency (Fig. 2d) indicates that another process must be overcome for the successful development of an efficient siRNA delivery system.

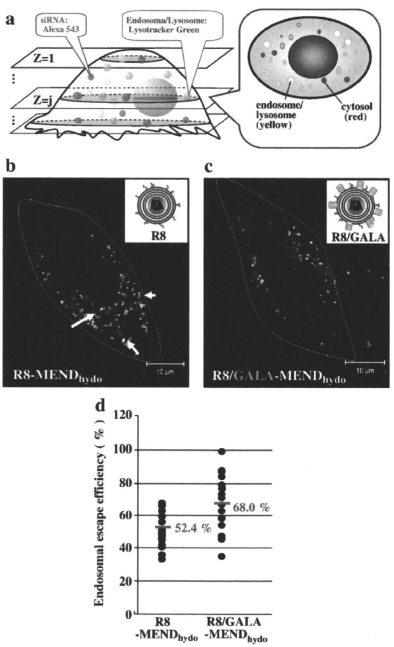

Fig. 2. Evaluation of endosomal escape efficiencies of siRNA. Evaluation of endosomal escape efficiency of MENDs. a. Schematic diagram illustrating the quantitative evaluation system used to evaluate endosomal escape. MENDs prepared with Alexa546-labeled siRNA were transfected to HeLa-GL3 cells. The endosomes/lysosomes were stained with Lysotracker green to discriminate between pDNA in endosomes/lysosomes and the cytosol. The fraction of siRNA in endosomes and the cytosol was quantified based on the pixel area of clusters in each region of interest, as described in Methods. b–c. Typical confocal image of intracellular trafficking of R8-MEND$_{hydo}$ with (c) or without (b) GALA modification. White lines indicate the cellular region. Green, red and yellow (indicated by arrowhead) represents endosome/lysosome, siRNA in the cytoplasm and siRNA in endosomes/lysosomes, respectively. d. Quantitative comparison of endosome escape efficiency between GALA-modified and unmodified R8-MEND$_{hydo}$. Endosome escape efficiency in 15 individual cells was plotted.

3.3. Evaluation of cellular uptake and intracellular dissociation efficiency

It is postulated that cytoplasmic dissociation process of siRNA is also rate-limiting for its function. The dissociation efficiency of siRNA in R8/GALA-MEND$_{hydo}$ was quantified by CIDIQ analysis (Fig. 3a). Alexa546-labeled siRNA was loaded in the MEND$_{hydo}$, with a labeling of lipid envelope by 1 mol% NBD. The dually labeled R8/GALA-MEND$_{hydo}$ was transfected, and a Z-series of confocal images were then captured at 9 h post-transfection (Fig. 3a). siRNA in loaded and dissociated form were detected as yellow clusters and red clusters, respectively (Fig. 3b). The pixel areas corresponding to the red and yellow clusters were integrated using all of the Z-series of confocal images (S(red) and S(yellow), respectively). Dissociation efficiency was denoted as the percentage of S (red) to the total of the S(red) and S(yellow) clusters. Quantification of the pixel areas of the clusters indicated that only 56% of the siRNA was dissociated in the R8/GALA-MEND$_{hydo}$ (Fig. 3d). In contrast, almost all of the siRNA were detected as red clusters in the case of the R8/GALA-MEND$_{SUV}$ (Fig. 3c). A quantitative evaluation indicated that the dissociation efficiency for the R8/GALA-MEND$_{SUV}$ was approximately 90% (Fig. 3d). Furthermore, the dissociation efficiency was homogenous over the cell population. A FACS analysis revealed that the cellular uptake varied substantially from one cell to another in R8-MEND$_{hydo}$ and R8/GALA-MEND$_{hydo}$. On the other hand, the cellular uptake efficiencies for the MEND$_{SUV}$ were slightly higher (at maximum of 2-fold by geo mean calculation) and more homogeneous for individual cells. Collectively, controlling the number of lipid layers is an advantage, in terms of improving dissociation efficiency, and for overcoming heterogeneity in the cellular uptake process (Fig. 3d and e).

3.4. Delivery of anti-SOCS1 siRNA to BMDCs for cancer immunotherapy

To investigate the utility of the R8/GALA-MEND$_{SUV}$ in the delivery of therapeutic siRNAs, we examined the biological response of a gene knockdown targeting SOCS1 in mouse bone marrow-derived dendritic cells (BMDCs). In order to confirm the RNAi efficacy in these cells, anti-GAPDH siRNA was transfected to BMDCs for 24 h. The R8/GALA-MEND$_{SUV}$ was able to suppress GAPDH expression more prominently than LFN2000 (Supplemental Fig. 1). We subsequently examined the silencing effect against SOCS1 following induction by IFN-γ. As shown in Fig. 4a, SOCS1 mRNA was reduced to 21.5% of the levels of non-treated BMDCs. As expected, BMDCs transfected with anti-SOCS1 were more responsive to IFN-γ than those transfected

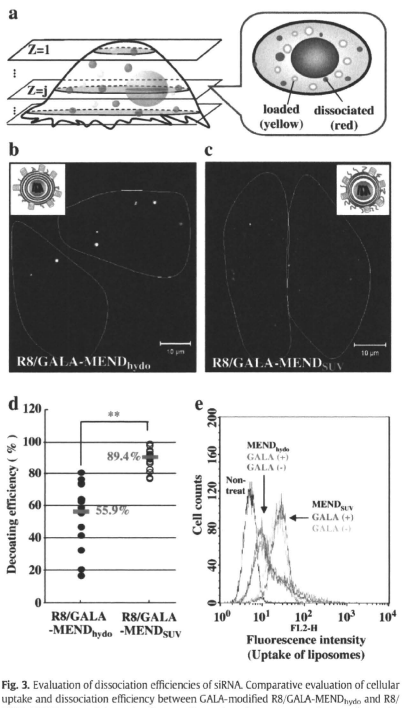

Fig. 3. Evaluation of dissociation efficiencies of siRNA. Comparative evaluation of cellular uptake and dissociation efficiency between GALA-modified R8/GALA-MEND$_{hydo}$ and R8/GALA-MEND$_{SUV}$. a. Schematic diagram illustrating the system used to evaluate the dissociation process. MENDs were prepared with Alexa546-labeled siRNA. The lipid envelope was labeled by incorporation of an NBD-labeled lipid. Fraction of siRNA in the dissociated form was quantified based on the pixel area of clusters in each region of interest as described in Methods. b–c. Typical confocal images of R8/GALA-MEND$_{hydo}$ (b) and R8/GALA-MEND$_{SUV}$ (c). White lines indicate the cellular region. Red and yellow clusters represent dissociated and loaded siRNA, respectively. d. Comparison of dissociation efficiency between R8/GALA-MEND$_{hydo}$ and R8/GALA-MEND$_{SUV}$. Dissociation efficiency in 15 individual cells was plotted. e. Evaluation of the cellular uptake of siRNA introduced by a conventional MEND$_{hydo}$ and the MEND$_{SUV}$. MENDs loading Alexa546-labeled siRNA were incubated with HeLa-GL3 cells for 1 h, and then subjected to flow cytometry.

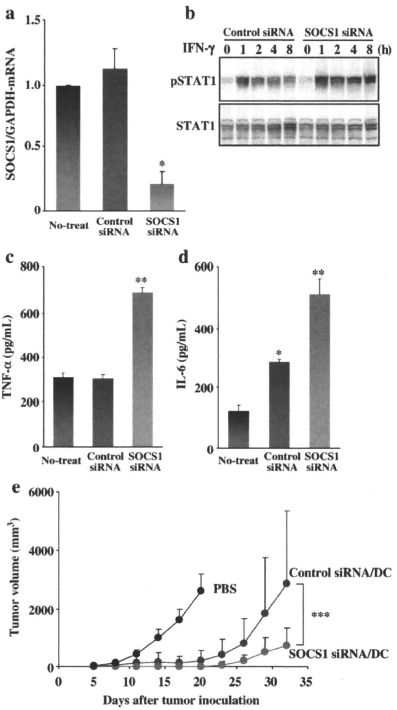

Fig. 4. SOCS1 gene silencing and antitumor activity. SOCS1 gene silencing and enhancement of antitumor activity of dendritic cells mediated by R8/GALA-MEND$_{SUV}$. a. Gene silencing of SOCS1. BMDCs were transfected with anti-SOCS1 siRNA or negative control siRNA. Six hours after transfection, the cells were stimulated with IFN-γ for 24 h and assayed for mRNA expression by quantitative RT-PCR. SOCS1 levels were normalized to non-treated BMDCs. Data are mean ± S.D. of three independent experiments. *P<0.005 vs. Control siRNA. b. STAT1 tyrosine phosphorylation in anti-SOCS1 siRNA or negative control siRNA-transfected BMDCs stimulated with IFN-γ was analyzed by Western blotting. c–d. TNF-α (c) and IL-6 (d) concentrations in the culture supernatants were determined by ELISA at 24 h after stimulation with IFN-γ. Data are the mean ± S.D. of three independent experiments. *P<0.005, **P<0.001 vs. non-treated BMDCs. e. Inhibition of E.G.7-OVA tumor growth by SOCS1-silenced BMDCs immunization. C57BL/6 mice (4 mice/group) were immunized with 3.8×10^5 siRNA-transfected, OVA-pulsed BMDCs. One week after DC immunization, 8×10^5 tumor cells were inoculated s.c. and tumor size was measured at 3 day intervals. ***P<0.005 vs. Control siRNA/DC.

with control siRNA, as evidenced by the enhanced and prolonged phosphorylation of STAT1 (Fig. 4b). Consistent with these data, higher levels of proinflammatory cytokines (i.e. TNF-α and IL-6) were produced by the SOCS1-silenced BMDCs upon stimulation (Fig. 4c and d, respectively). We observed a slight increase in IL-6 production by BMDCs transfected with control siRNA. This is probably due to sequence-dependent non-specific stimulation by siRNA transfection, since a similar increase in IL-6 was also observed with different siRNAs.

The effect of SOCS1 knockdown on the ability of BMDCs to induce antitumor immunity was then examined (Fig. 4e). BMDCs transfected with SOCS1-targeting or control siRNA were pulsed with an antigen (OVA). These pulsed BMDCs are activated by adjuvant (LPS), and then pre-immunized to C57BL/6 mouse. These mice were challenged with E.G.7-OVA tumor cells one week after the immunization. BMDCs vaccination effectively retarded tumor growth regardless of SOCS1 knockdown compared with control mice treated with PBS until 20 days. After a longer evaluation, however, SOCS1-silenced BMDCs were more potent in suppressing tumor growth compared to the control BMDCs. These results show that siRNA loaded in R8/GALA-